North American Upstream Feature-Resolving and Tropopause Uncertainty Reconnaissance Experiment (NURTURE)

Concept Paper submitted to Will McCarty at NASA Headquarters

Figure 1: Waves crashing on a northern France pier during storm Ciara in January 2020. Image credit: New York Times.

Authors: Steven Cavallo[1], Chris Davis[2], James Doyle[3], Andrea Lang[4], Lynn McMurdie[5], Ryan Torn[6], David Parsons[1], Andrew Winters[7]

[1] University of Oklahoma, School of Meteorology
[2] National Science Foundation National Center for Atmospheric Research, Mesoscale and Microscale Meteorology Laboratory
[3] Naval Research Laboratory, Marine Meteorology Division
[4] University at Albany, State University of New York, Department of Atmospheric and Environmental Sciences and University of Wisconsin–Madison, Department of Atmospheric and Oceanic Sciences
[5] University of Washington, Department of Atmospheric Sciences
[6] University at Albany, State University of New York, Department of Atmospheric and Environmental Sciences
[7] University of Colorado, Boulder, Department of Atmospheric and Oceanic Sciences

Table of Contents

1. NURTURE Overview

The North American Upstream Feature-Resolving and Tropopause Uncertainty Reconnaissance Experiment (NURTURE) is a conceptualized field campaign designed to advance knowledge of the processes that lead to extreme high-impact weather (HIW) events during the winter, such as severe cold air outbreaks, windstorms and hazardous seas, sea ice breakup, and extreme precipitation. It will be the first NASA airborne experiment utilizing the NASA Boeing 777 aircraft and will nominally be based in Gander, Newfoundland and Labrador, Canada. The experiment is planned to take place during January and February 2026. The scientific pursuits of NURTURE aim to measure:

(1) The dynamical and physical processes that control upstream perturbations to the jet stream, such as tropopause polar vortices, dry air intrusions, turbulence, and their interactions with the jet stream,
(2) Upper tropospheric and lower stratospheric influences on tropopause structure and jet stream dynamics, and
(3) The boundary-layer processes that facilitate communication between the troposphere and surface and that precondition the environment for HIW events.

The overarching goal of NURTURE is to quantify the impact that perturbations poleward of the jet stream have on jet stream variability and HIW events. This goal will be accomplished by addressing the following science questions:

- **Science Focus 1: Tropopause Structure and Dynamics.**
  - **Science Question 1.1:** What are the diabatic and kinematic processes governing the development and maintenance of Tropopause Polar Vortices (TPVs)?
  - **Science Question 1.2:** How does jet stream amplification occur in the presence of TPVs, and what are the implications for downstream HIW?
- **Science Focus 2: Diabatic Processes.**
  - **Science Question 2.1:** How does moisture impact the diabatic processes important for determining the three-dimensional structure in the upper troposphere and lower stratosphere (UTLS) in the vicinity of TPVs and the polar jet stream?
- **Science Focus 3: Upper Troposphere and Lower Stratosphere / Boundary Layer Interactions.**
  - **Science Question 3.1:** How do processes related to TPVs generate cold continental airmasses and that lead to cold air outbreaks?
  - **Science Question 3.2:** How do cold continental air masses evolve over maritime regions and feed back to UTLS structure?

Answering the above science questions will address how processes that start at sub- mesoscales translate to synoptic and large scales, resulting in HIW events that impact regions often far from the origin of disturbances responsible for these events. ***The study of multi-scale processes and lifecycles of important atmospheric features requires the NASA 777's long-range and substantial payload capacity, making it an ideal aircraft for meeting the objectives of NURTURE.*** The measurement strategy of NURTURE focuses on long-range, system-following aircraft missions that probe the upper-troposphere and lower-stratosphere (UTLS) region to quantify its structure through kinematic, thermodynamic and constituent measurements, as well as the deep tropospheric measurements over maritime regions to assess evolution of the boundary-layer and free troposphere in response to cold air extrusions. NURTURE emphasizes the life cycles of mesoscale and synoptic-scale disturbances of Arctic origin, and how their juxtaposition with mid-latitude features creates high-impact weather. It also targets measurements that are needed to reduce systematic process errors in numerical models within the UTLS and maritime tropospheric regions in the vicinity of features responsible for HIW.

Some of the important features and processes of interest in NURTURE are highlighted in Figure 2. TPVs are one of the mesoscale features important for forming surface cyclones. In the Arctic, these surface cyclones are referred to as Arctic Cyclones, and can sometimes become the largest and longest-lived surface cyclones on the planet. Locally, the strong winds from Arctic Cyclones can result in devastating and long-lasting impacts in the Arctic, such as severe coastal erosion and the very rapid breakup of sea ice. TPVs, which are precursors to Arctic Cyclones, tend to form mostly in the Canadian Archipelago region of North America. Once TPVs form, they can intensify for long periods and are characterized by the formation of a cold air mass directly beneath them and a dry air intrusion in the upper-troposphere. Occasionally, TPVs can be influenced by larger-scale flow patterns and move equatorward, where the cold-air masses and dry-air intrusions accompany them. Observations indicate that TPVs can merge with the jet stream, creating a local region of high wind speeds that produces favorable conditions for downstream HIW events via the formation of extreme extratropical surface cyclones. While it is often observed that a TPV can merge into the jet stream, there are also times that this does not occur. The exact physical and dynamical processes that determine whether this merging will occur are not currently known. Moreover, the progression of TPVs to maritime regions often results in markedly increased surface fluxes of heat and moisture. The rapid adjustment of the troposphere in response may have large consequences for the dynamic tropopause, which can reside at or below 600 hPa in some cases, but the linkage between boundary layer processes and the lowered tropopause is relatively unexplored, as are its downstream consequences.

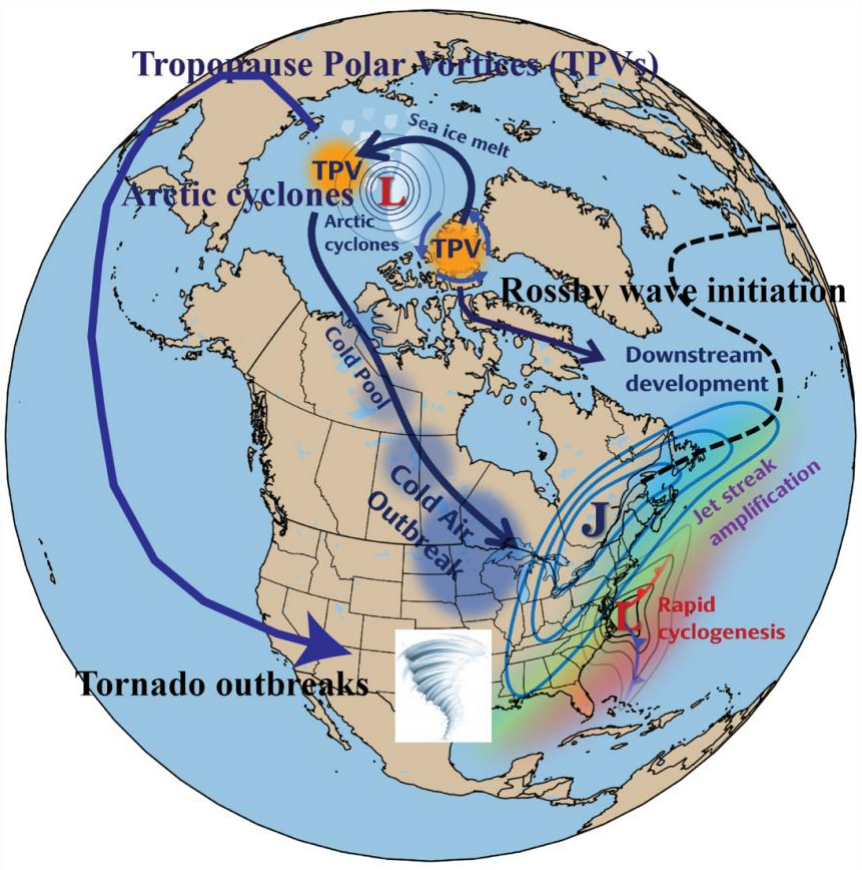

Figure 2: Conceptual schematic of an idealized TPV life cycle and impacts in the Northern Hemisphere. TPVs commonly form in northeastern Canada and can contribute to Arctic cyclone intensification, which can result in a decrease in sea ice extent. TPVs can then enter the midlatitudes, leading to various impacts, including cold air outbreaks, rapid cyclogenesis, jet streak amplification, and downstream Rossby wave initiation.

2. Introduction

1.1. High Impact Weather (HIW)

High-impact weather (HIW) events are responsible for an increasing trend in the frequency of billions-dollar disasters (USD) during the last 40 years. In particular, an average of 8.1 billion-dollar events per year impacted the U.S. during 1980–2022 after adjusting for inflation, with that number rising to an average of 18.0 events when considering the most recent 5-year period, 2018–2022 (NCEI 2023). Cold season HIW events are often tied to surface cyclones and anticyclones (e.g., Röthlisberger et al. 2016). In particular, widespread wind and precipitation extremes develop near surface cyclones and their attendant frontal boundaries (e.g., Bosart et al. 1996; Ralph et al. 2006; Dacre et al. 2015; Moore et al. 2015, 2019, 2020; Pohorsky et al. 2019; Bentley et al. 2019), whereas temperature extremes are induced via the transport of anomalous temperatures induced by the circulations accompanying surface cyclones and anticyclones (e.g., Colle and Mass 1995; Westby et al. 2013; Westby and Black 2015; Grotjahn and Zhang 2017; Xie et al. 2017; Winters et al. 2019; Biernat et al. 2021). Surface cyclogenesis and anticyclogenesis are strongly coupled to the state and evolution of the upper-tropospheric jet stream (e.g., Chang et al. 2002; Lehmann and Coumou 2015; Bosart et al. 2017; Röthlisberger et al. 2016; Winters and Attard 2022). Namely, along-jet variations in flow speed and curvature induce ageostrophic circulations within the near-jet environment that support cyclogenesis and anticyclogenesis along baroclinic zones beneath the jet (e.g., Namias and Clapp 1949; Palmén and Newton 1969; Keyser and Shapiro 1986; Uccellini et al. 1984; Sanders and Hoskins 1990). **Consequently, observing the multiscale processes that govern the evolution and intensity of upper-tropospheric jet streaks is essential for understanding the development of cold season HIW events.**

1.2. Ingredients to HIW

1.2.1: Upper-Tropospheric and Lower Stratospheric Processes

The upper troposphere and lower stratospheric (UTLS) region plays an important role in the evolution of weather and climate. The UTLS region contains the tropopause boundary between the relatively moist and less statically stable troposphere and the relatively dry, ozone rich, statically stable lower stratosphere. In the UTLS region, the jet streams associated with HIW events are characterized by strong gradients of potential vorticity (PV) along isentropic surfaces intersecting the tropopause. These PV gradients act as a waveguide for propagating Rossby waves (Hoskins and Ambrizzi 1993; Schwierz et al. 2004; Martius et al. 2010) that can spawn HIW events thousands of kilometers downstream through the propagation of disturbance energy in the form of Rossby wave packets (Wirth et al. 2018). Rossby waves can propagate within the UTLS region where they are subject to the dispersive nature of waves, meaning they can be transmitted, absorbed, reflected, or refracted in three dimensions, contingent with their wavenumber and the profiles of temperature and wind near the tropopause. The tropopause structure is an important aspect of jet streams and storm track location and strength, and it is well correlated to Rossby wave amplitude and dispersion. Boljka and Birner (2022) show that the extratropical tropopause inversion layer, on the poleward side of the jet, is well correlated to tropopause sharpness. A sharper tropopause

structure promotes an intensified general circulation and an equatorward shifted jet on longer timescales and on shorter timescales, it can impact the evolution of individual wave features on the waveguide.

While the timescale of variability in the troposphere is on the order of days, variability in the stratosphere generally occurs on subseasonal-to-seasonal (S2S) timescales of weeks, making the UTLS region an important region to resolve for successful extended range predictions. In the wintertime, stratospheric variability in the Northern Hemisphere polar vortex can be communicated down through the UTLS region and is known to have S2S timescale impacts on the midlatitude storm tracks (e.g., Gray et al. 2018; Attard and Lang 2019), weather regimes (e.g., Domeisen et al. 2020; Charlton-Perez et al. 2018), and extratropical temperature extremes (e.g., Tripathi et al. 2015; Butler et al. 2019; Matthias and Kretchmer 2020). After both strong and weak stratospheric vortex events, temperature and momentum anomalies persist in the lower stratosphere for up to 60 days where they impact the PV structure within the UTLS region and influence the evolution of extratropical weather systems and storm tracks. Likewise, the impacts of tropospheric processes can change the tropopause structure from below. Diabatic processes, like those in cyclones, warm conveyor belts, and atmospheric rivers, as well as radiative processes from cloud ice and liquid water, and water vapor are important in restructuring or reconfiguration of the tropopause-level PV (e.g., Harvey et al. 2020, Cavallo and Hakim 2013).

Moisture biases in the lower stratosphere can lead to biases in the tropopause sharpness and structure, including positive biases in tropopause height, a cold bias in the lower stratosphere and a warm bias in the upper troposphere (e.g., Bland et al. 2021). These systematic biases act to weaken the representation of TPVs and the waveguide in the extratropics (Fig. 3). The observations of the extratropical wintertime UTLS region will serve several roles that can lead to a reduction in systematic model biases. First, observations of wind and temperature in the high-latitude UTLS region, in locations away from the midlatitude jet stream, will serve to assess the horizontal and vertical gradients that contribute to the Arctic tropopause sharpness and structure on the poleward side of the jet for a given stratospheric vortex state. In addition, the observation of water vapor, ozone, and cloud ice and water content will inform the assessment of the in-situ maintenance of high-latitude tropopause sharpness from thermodynamic processes. Near the midlatitude jet stream, observation of these same variables on the polar and midlatitude side of the jet stream will serve to reduce the biases in tropopause vertical and horizontal structure in the development of jet streaks and during waveguide amplification. More specifically. These observations will follow the evolution and contribution of the high-latitude UTLS structures in the development of UTLS precursors to high impact weather.

1.2.2. Tropopause Polar Vortices

Tropopause polar vortices (TPVs) are coherent sub-synoptic scale vortices of the UTLS region that are characterized by cold air masses underneath them near the surface. TPVs mainly possess radii of several hundred to one thousand kilometers and can persist at timescales of months (Hakim 2000; Hakim and Canavan 2005; Cavallo and Hakim 2009, 2012; Bray and Cavallo 2022; Gordon et al. 2023). Emerging research suggests that cool-season TPV intensity and location vary on S2S timescales with the state of the stratosphere (Figure 3) however, most current knowledge of TPVs is restricted to when TPVs are isolated from the jet stream. Recently, TPV studies have shown that while they generally form and intensify in polar regions, they are associated with lower-latitude extreme cold air outbreaks (Papritz et al. 2019; Biernat et al. 2021; Lillo et al. 2021) and tornado outbreaks in the continental United States (Bray et al. 2021). Even

before TPVs exit polar regions, TPVs have been noted to play important roles in the development and evolution of Arctic Cyclones (Yamagami et al. 2017; Bland et al. 2021), and very rapid reductions in Arctic sea ice have been noted to occur in association with Arctic cyclones (Simmonds and Rudeva 2012; Zhang et al. 2013; Blanchard-Wrigglesworth et al. 2022). The loss of Arctic sea ice increases the potential for shipping in the Arctic due to increased accessibility and shorter shipping routes (Mudryk et al. 2021; Li and Lynch 2023) and has also led to severe coastal erosion issues that pose the possibility of relocating coastal communities (Barnhart et al. 2016; Fang et al. 2018).

Diabatic heating due to longwave (LW) radiative clear-sky cooling is the primary process responsible for strengthening TPVs (Cavallo and Hakim 2013). The direct effects of latent heating play a destructive role in TPV intensification. In polar regions, where TPVs and cold air masses originate, latent heating rates are relatively low compared to the rest of the globe due to the low saturation moisture content at cooler temperatures. While latent heating effects can have a significant impact on TPV intensity, the effects of latent heating in polar regions are much smaller than the effects of LW radiative cooling that strengthen TPVs, in contrast to midlatitude or tropical regions where latent heating effects are generally stronger than radiative cooling effects.

Cavallo and Hakim (2013) found that most of the TPV intensification occurs in clear-sky conditions due to a locally enhanced vertical water vapor gradient in the vortex core. This gradient is locally stronger in the TPV core beneath the tropopause due to the downward intrusion of dry stratospheric air characterized by the lower tropopause inside the vortex core relative to the surrounding environment. Occasionally, if clouds are present in the upper troposphere, cloud-top radiative cooling further enhances TPV intensification. The additional intensification from clouds also strongly depends on the phase of the clouds, where mixed-phase or liquid-phase clouds can increase radiative cooling rates by an order-of-magnitude above cloud tops and more rapidly intensify a TPV (Turner et al. 2018; Borg et al. 2020).

TPVs are often noted as a precursor to surface cyclones in the midlatitudes (Uccellini et al. 1985; Sanders 1986; Bosart et al. 1996). The conditions that provide a favorable environment for generating surface cyclones and their associated extreme weather are dynamically related to jet streaks. Hakim (2000) showed that the intensity of tropopause-based potential vorticity (PV) anomalies is directly related to jet streak velocity. Pyle et al. (2004) validated this relationship, providing multiple examples of jet streak intensification in the presence of tropopause-based PV anomalies confined to periods of close proximity between the jet streak and PV anomaly.

Climatologically, the strongest jet streaks over the North Atlantic (i.e., those that exceed 100 m s^{-1}) occur during December–February, reside downstream of local maxima in TPV frequency over northeastern Canada, and are frequently characterized by polar-subtropical jet superpositions (Fig. 10; Christenson et al. 2017; Winters 2021). Conceptually, these strong jet streaks develop when polar-based cyclonic PV anomalies, such as a TPV, and tropical-based anticyclonic PV anomalies become meridionally juxtaposed at midlatitudes. This juxtaposition leads to a sharpening of the potential temperature gradient along the tropopause and an acceleration of jet wind speeds (Fig. 2). Tropical-based anticyclonic PV anomalies arise due to the poleward transport of low-PV, upper-tropospheric air towards midlatitudes, as well as via midtropospheric diabatic heating in the vicinity of strong tropical and extratropical cyclones (e.g., Iskenderian 1995; Morgan and Nielsen-Gammon 1998; Ahmadi-Givi et al. 2004; Grams et al. 2011;

Fröhlich et al. 2013; Archambault et al. 2013, 2015; Winters and Martin 2016). The interaction between polar-based cyclonic PV anomalies with tropical-based anticyclonic PV anomalies indicates a dynamical and thermodynamic environment conducive to high-impact weather.

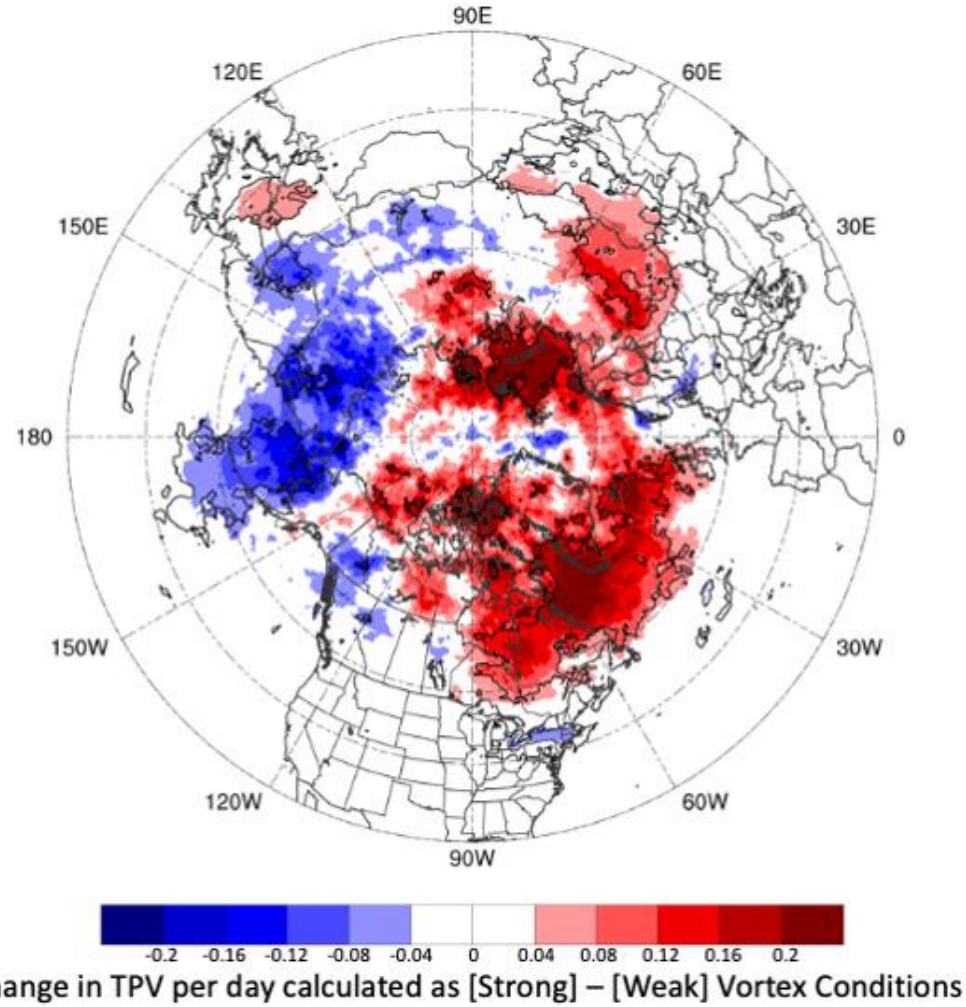

Figure 3: The TPV frequency difference between periods of strong stratospheric vortex conditions and weak stratospheric vortex conditions, where strong (>90%) and weak (< 10%) vortex conditions are calculated as the 7-day running mean of the 60˚N zonal-mean zonal wind at 10 hPa during the winter (DJF) 1979/80-2017/18 period in the ERA-Interim reanalysis.

1.2.3. Jet Superpositions

As discussed above, the formation of an anomalously strong jet streak can result from a polar-subtropical jet superposition . (e.g., Winters and Martin 2014, 2016, 2017; Handlos and Martin 2016, 2021; Christenson et al. 2017; Winters et al. 2020 a,b). The leading characteristics of a jet superposition include anomalously strong wind speeds that may exceed 100 m s^{-1}, a steep, single-step pole-to-equator tropopause structure, and the consolidation of the pole-to-equator baroclinicity into a narrow zone of contrast in the vicinity of the jet. The development of enhanced baroclinicity during a jet superposition is accompanied by a vigorous across-jet ageostrophic circulation that lies within a vertical plane perpendicular to the jet. This ageostrophic

circulation provides a mechanism through which jet superpositions can directly influence HIW events. For example, surface cyclones that develop in association with North American jet superpositions are significantly stronger relative to the average cold-season cyclone, 64% of jet superpositions feature widespread extreme precipitation within the near-jet environment, and 68% of jet superpositions are accompanied by widespread extreme near-surface winds (Reiher and Winters 2024).

Model representations of jet superposition dynamics are reliant on accurate depictions of the physical features and processes that facilitate a superposed jet, such as TPV mergers with the poleward flank of the jet, as well as latent heating and divergent outflow on the equatorward flank of the jet. With respect to the former, the superposed jet structure is dependent on an accurate representation of polar-based cyclonic PV anomalies poleward of the jet, such as TPVs. Such features can be misrepresented in models due to aforementioned errors in lower-stratospheric radiative cooling (Qu et al. 2020; Woiwode et al. 2020; Bland et al. 2021) that subsequently influence the tropopause slope. Gray et al. (2014) also note that forecast models have a tendency to relax the magnitude of the horizontal PV gradient near the tropopause. In the context of jet superpositions, which feature extremely sharp horizontal PV gradients, this tendency can impact the forecasted jet intensity, the downstream propagation of Rossby waves, and the resultant capability for the jet to induce downstream sensible weather impacts. Improved observations of tropopause-based disturbances and dynamical processes that modulate the tropopause structure as part of NURTURE are essential for improved understanding of the formation of jet superpositions, their evolution, and their capability to induce high-impact weather.

1.2.4. Cold Air Outbreaks

Extreme cold air outbreaks (CAOs) are frequently known to cause significant economic losses and disruptions to travel and often lead to fatalities (Huang et al. 2021). For instance, the severe CAO in the southern Great Plains of the United States in February 2021 caused over 262 deaths, with millions of power outages, and over $26.5B in economic damage (NOAA 2021). This single event caused damages totaling more than the combined average annual cost and number of fatalities from tropical cyclones and severe thunderstorms in the United States. It is, therefore, of great importance to learn more about the processes that cause CAOs so that predictions can be made in both the short- and long-term to aid in decision-making and climate adaptation.

The formation and air mass modification of cold air masses over continental polar regions remains an outstanding question. Current knowledge dates to numerous studies showing the significance of how cold air masses deepen through microphysical-radiative processes occurring over relatively cold surfaces often covered by snow or ice (e.g., Wexler 1936; Byers et al. 1951; Curry 1983; Curry 1987). More recently, studies have been linking these cold air masses to cyclonic tropopause polar vortices (TPVs), which are often associated with extreme cold air outbreaks when a TPV moves south from the Arctic into the midlatitudes (Papritz et al. 2019; Biernat et al. 2021; Lillo et al. 2021; Xi et al. 2023). The physical linkage between lower levels to the tropopause is illustrated in studies such as Hoskins et al. (1985) and Thorpe (1986), showing that a cyclonic circulation at the tropopause level balances a cold anticyclone at the surface. Figure 4 shows how a cold air mass at the surface can be linked to a TPV. When TPVs strengthen, they are typically located in high latitudes and isolated from the jet stream (Figure 4a). TPVs are characterized by a cyclonic PV anomaly near the tropopause, which is accompanied by a cold air anomaly directly underneath the TPV. As the TPV strengthens, the cyclonic PV anomaly strengthens, therefore

strengthening the magnitude of the cold air mass at the surface (i.e., the cold pool). The larger-scale atmospheric flow can interact with the smaller-scale TPV and advect the TPV and cold pool equatorward (Figure 4b). As the cold pool moves equatorward, the cold anomaly strengthens substantially due to the fact that the further removed the cold air mass is from its origin in high latitudes, the less frequent such cold air masses are likely to be experienced at any given location in lower latitudes. Additionally, cold domes can be advected far away from the TPV, for instance, when there is a larger-scale blocked flow pattern, or significant topography to enhance the equatorward advection of the cold dome.

Recent systematic studies examined TPV-CAO linkages in northern Europe (Papritz et al. 2019) and North America (Biernat et al. 2021). For CAOs originating in the Fram Strait, Papritz (2019) found that 29% of the top 100 CAOs are associated with a TPV, which increases to 40% of the top 40 CAOs. This compares to a 14.5% probability of a TPV within the same region for any randomly chosen day, implying a statistical linkage between CAOs and TPVs. Over North America, (Biernat et al. 2021) found a spatial correlation between the density of TPV and cold pools transported into the midlatitudes. Roughly 32-35% of CAOs are linked to cold pools associated with TPVs over the northern United States, decreasing to 4-12% over the southern United States. Along with (Lillo et al. 2021), these three studies indicate that while a statistical linkage exists between TPVs and CAOs, their characteristics differ by geographic region.

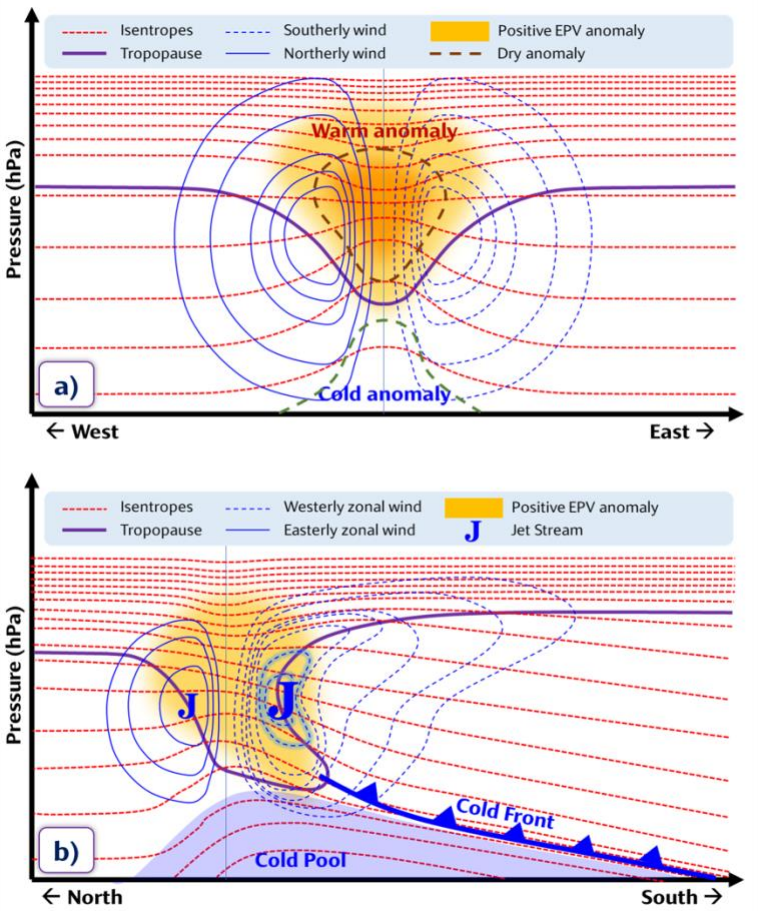

Figure 4: Idealized cross section schematic through (a) an isolated TPV in high latitudes, and (b) a TPV interacting with a midlatitude jet streak and associated with a cold air outbreak.

1.2.5. Diabatic Heating

Diabatic heating associated with cyclones on the warm side of the jet can have a substantial impact on both the amplitude and the structure of the jet. This can come in the form of Rossby waves that can propagate along steep gradients in the tropopause, for which the jet stream is an example. Perturbations to the waveguide related to cyclones have been shown to act as a Rossby-wave generator, mainly through the divergence in the upper-tropospheric wind in a region adjacent to the sloping tropopause. Strong upper-level divergence is largely associated with latent heat release due to condensation (e.g., Davis et al. 1993; Riemer et al. 2008; Riemer and Jones 2010, 2014; Quinting and Jones 2016), which is often linked to the diabatic processes within the warm conveyor belt (WCB; Green et al. 1966; Browning 1971; Harrold 1973; Carlson 1980) of extratropical cyclones. As a result, several studies have hypothesized that Rossby wave forecasts are modulated by upstream diabatic processes associated with the transport of relatively warm and moist air poleward and upward within the WCB (e.g., Grams et al. 2011; Teubler and Riemer 2016; Baumgart et al. 2018; Berman and Torn 2019).

Poor downstream forecasts have been traced to the representation of processes associated with latent heat release and hence downstream forecast variability (e.g., Grams et al. 2018; Martínez-Alvarado et al. 2016). These errors could be related to errors in microphysical processes (e.g., Joos and Wernli 2012), and lower-tropospheric moisture supply (Schafler and Harnisch 2015; Berman and Torn 2019; Berman and Torn 2022). One way to quantify the role of WCBs on Rossby wave and jet stream forecasts is the PV tendency partitioning technique such as was employed by Teubler and Riemer (2016). For instance, Baumgart et al. (2018) applied the PV tendency technique to an ECMWF forecast of a PV ridge, which indicated that tropopause-based PV anomalies had a larger contribution to PV error growth than that of upper-tropospheric divergent outflow related to an upstream WCB. These results describe an upstream growth paradigm whereby unbalanced errors in latent heating grow upscale, perturb the jet and waveguide and yield synoptic and planetary-scale errors as the differences act upon synoptic features and cause downstream differences (e.g., Zheng et al. 2007; Rodwell et al. 2013; Baumgart et al. 2019). For example, the aforementioned diabatic processes frequently contribute to jet superposition development (e.g., Winters et al. 2016; Winters et al. 2020a). Therefore, errors in the representation of these processes can influence the resultant superposed jet structure and its ability to induce HIW.

3. Science Focus Areas

The previous section highlights the multiscale processes that can influence the jet stream and its relationship to HIW. These processes telescope down from S2S variations in the lower-stratospheric polar vortex, to the dynamics of synoptic-scale waves, surface cyclones, and TPVs, to mesoscale circulations within the near-jet environment, and to sensible heat and moisture fluxes within the boundary layer. Improved understanding of these multiscale processes, their interaction, and their influence on HIW, require detailed observations that illuminate the underlying dynamics at play as well as biases in their representation within numerical weather prediction models and long-term gridded datasets. **In line with this requirement, the primary objective of NURTURE is to quantify the influence of perturbations poleward of the jet on jet stream variability and the development of HIW.** Under this objective, three science focus areas for NURTURE are identified: (1) tropopause structure and dynamics, (2) diabatic processes, and (3)

UTLS/boundary layer interactions. Key science questions and hypotheses that fall under these focus areas are summarized in Figure 5.

3.1. Science Focus 1: Tropopause Structure and Dynamics

The equatorward transport of TPVs is a frequent precursor to the development of anomalously-strong jet streaks and HIW (Pyle et al. 2004; Winters 2021). **Consequently, the scientific aims of NURTURE are to observe the evolution of TPVs prior to their merger with the jet, as well as their resultant influence on jet structure and dynamics.** NURTURE intensive observation periods (IOPs) will specifically target UTLS large-scale flow conditions that favor the transport of TPVs into close proximity to the midlatitude jet (H1.1), and document how flow deformation induces asymmetries in the structure of TPVs throughout their lifecycle (H1.3). These asymmetries are expected to impact mesoscale jet dynamics and the development of downstream HIW once TPVs merge with the jet (H1.2). Observational analyses will be focused on tracking the evolution of TPVs and their characteristics in the high latitudes prior to merging with the midlatitude jet, and on monitoring attendant changes in jet structure and dynamics when a TPV enters the midlatitudes. These observations are expected to increase knowledge of the high-latitude tropopause and TPV dynamics and characteristics, how TPVs accelerate jet wind speeds, and how mesoscale jet dynamics respond to the merger of a TPV.

3.2. Science Focus 2: Diabatic Processes

Diabatic processes include radiation and its dependence on cloud and water vapor variations, surface fluxes of heat and moisture (discussed below), and condensational heating through a range of vertical depths that helps connect the boundary layer and UTLS within regions of mesoscale ascent punctuated by shallow and deep moist convection. A key uncertainty that accompanies TPVs, their evolution, and their interaction with the jet is related to UTLS moisture biases (e.g., Bland et al. 2021). Such moisture biases are hypothesized to have a substantial effect on radiative processes near the tropopause, which affect the intensity of TPVs and the dynamic tropopause structure (Fig. 3). Accordingly, **NURTURE aims to observe the concentration of water vapor near TPVs and within the near-jet environment, investigate the source of water vapor in the UTLS, and examine the impact of water vapor on radiative processes near the tropopause.** In particular, analyses will focus on tracking the concentration of water vapor in the UTLS near TPVs and within the near-jet environment, and comparing those concentrations against output from reanalysis datasets and numerical weather prediction models. It is hypothesized that moisture biases within the UTLS lead to errors in longwave radiative processes, which locally modulate the distribution of potential vorticity and the dynamic tropopause structure (H2.1). Considered together, collective errors in boundary layer heat and moisture fluxes (see Sec. 3.3) and longwave radiative cooling in the troposphere are hypothesized to lead to inaccurate representations of the deep-tropospheric ascent regions. Divergence above such regions exerts a strong influence on the mesoscale jet structure. Furthermore, the character of secondary ageostrophic circulations facilitates surface cyclogenesis within the near-jet environment (H2.2). Systematic UTLS water vapor errors in numerical models are hypothesized to result from inaccurate representations of the cycling of water from boundary layer moisture fluxes, ascent through the troposphere, and eventual detrainment, plus the effect of radiative cooling on weak vertical circulations. The sources of

these systematic errors can be quantified using short-term forecast tendencies and analysis increments in an ensemble data assimilation framework (e.g., Klinker and Sardeshmukh 1992; Rodwell and Palmer 2007; Cavallo et al. 2016; Wong et al. 2020).

3.3. Science Focus 3: UTLS/Boundary Layer Interactions

TPVs are frequently accompanied by lower-tropospheric cold pools that induce CAOs across North America (Biernat et al. 2021; Lillo et al. 2021). The evolution of these cold pools as they migrate towards midlatitudes are subject to a spectrum of dynamical and thermodynamic processes, which introduce challenges in forecasting their characteristics. **NURTURE is designed to observe processes that generate and modify cold pools beneath TPVs as they translate from polar continental locations toward maritime areas.** Once these cold pools arrive over maritime regions, they are modified substantially via sensible and latent heat fluxes. These modified air masses subsequently interact with synoptic-scale flow features, such as atmospheric rivers, that can accompany surface cyclones developing within the near-jet environment. Observations over land will focus on tracking the development and evolution of cold pools that develop beneath TPVs. It is hypothesized that longwave radiational cooling near the UTLS over polar continental areas lowers the tropopause height and strengthens these lower-tropospheric cold pools (H3.1). Once cold pools move over maritime locations, their characteristics strongly depend on their path, translation speed, and the intensity of sensible and latent heat fluxes from the underlying surface (H3.2). In extreme situations, tropopause heights inside a mature TPV descend to near the top of the boundary layer. When a TPV moves over relatively warm open water, sensible heating, moist convection and latent heating are often initiated ahead of, and beneath, the TPV due to the decreasing atmospheric stability and simultaneous increase of lower-tropospheric water vapor. Conversely, the transport of relatively dry air from the UTLS to the boundary layer is also hypothesized to be sensitive to the representation of the dry air intrusion in the subsiding air inside, and beneath, the core of the TPV. NURTURE observations emphasize an improved representation of the thermodynamic environment accompanying lower-tropospheric cold pools, as well as their interaction with other flow features within the near-jet environment during HIW events (H3.3), connected by diabatic heating in the form of surface heat and moisture fluxes, condensational heating through the troposphere, and radiation. The linkage between the boundary layer and the UTLS is hypothesized to depend on the degree of moist static stability above the boundary layer; conditions of moist neutrality or instability being more favorable for a strong connection.

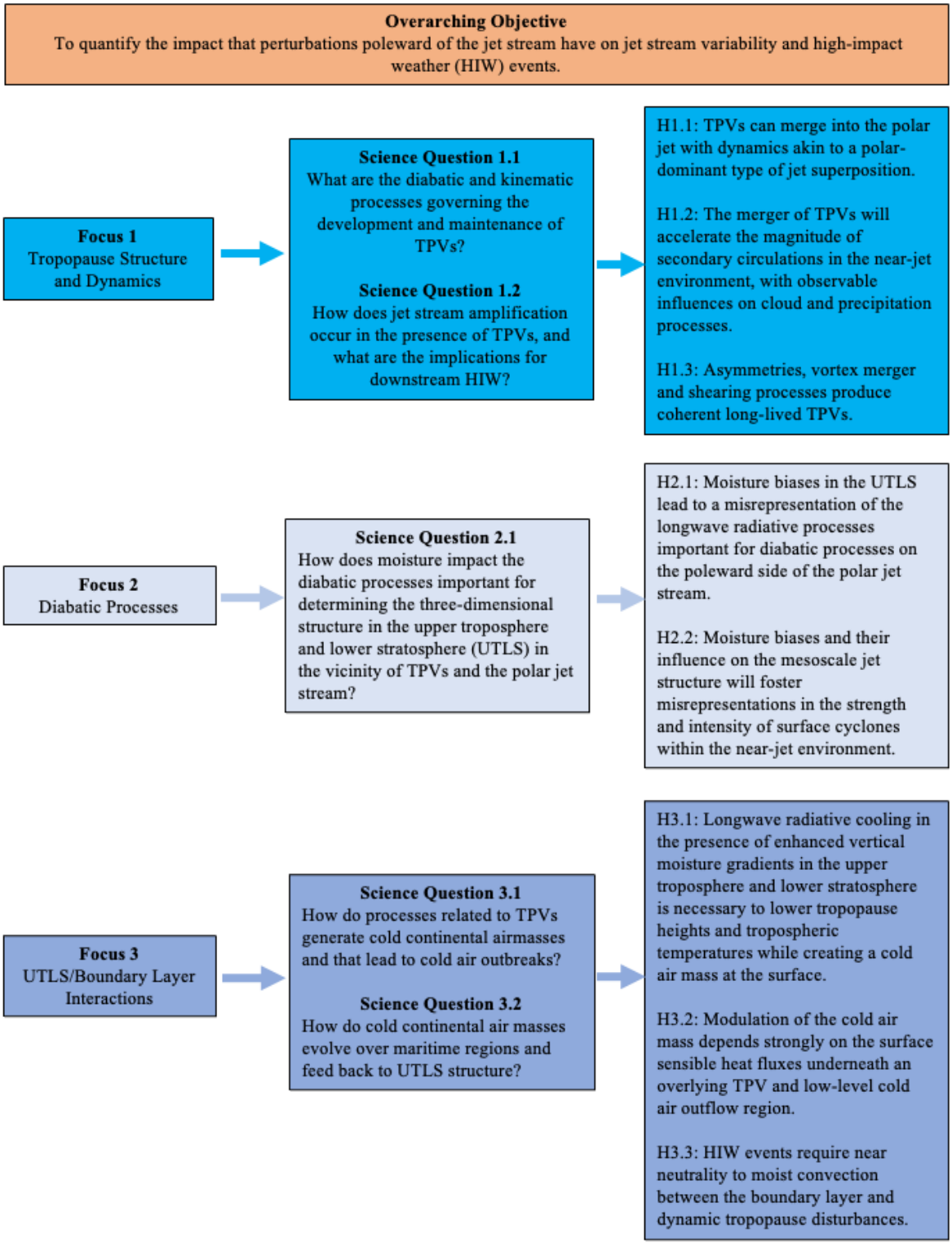

Figure 5: NURTURE science objectives.

4. Observations and Numerical Models

4.1. UTLS moisture and radiative uncertainties

Accurately representing mesoscale features in the UTLS poleward of the jet stream can be extremely challenging, given the relatively sparse in-situ upstream Arctic observations and limited amounts of moisture. This is compounded by the fact that the observations that do exist have inherent uncertainties and biases, which are especially pronounced at colder temperatures (Miloshevich et al. 2006; Ingleby 2017). For at least the past two decades, it has been well-established that atmospheric model analyses, re-analyses and forecasts are too moist in comparison to observations in the UTLS (Pope et al. 2001; Oikonomou and O'Neill 2006; Feist et al. 2007; Kunz et al. 2014; Dyroff et al. 2015; Woiwode et al. 2020) including the Global Forecasting System (Van Thien et al. 2010), Met Office Unified Model (Hardiman et al. 2015; Oh et al. 2018), and European Center for Medium Range Forecasting Integrated Forecasting System (Shepherd et al. 2018; Bland et al. 2021).

The effects of this moisture bias are illustrated in Figure 6a (Bland et al. 2021). A moisture bias in the UTLS centered around the tropopause would result in an erroneously large (small) decrease (increase) in water vapor with height above (below) the tropopause. Water vapor is an efficient emitter of longwave radiation; the result is too much cooling in the lower stratosphere. A steeper decrease in water vapor with height means less net absorption in this region. Likewise, the less steep decrease in water vapor with height in the upper troposphere would result in too much longwave absorption, erroneously heating the upper troposphere. Together, this results in the temperature dipole structure shown in Figure 6b, with a cool temperature bias in the lower stratosphere and a warm temperature bias in the upper troposphere.

TPVs are characterized by a warm temperature anomaly in the lower stratosphere and a cold temperature anomaly in the upper troposphere (Figure 6b). Cavallo and Hakim 2010, 2013 showed that there is an anomalous decrease (increase) of water vapor with height in the upper-tropospheric (lower-stratospheric) portion of TPVs that results in anomalous longwave radiative cooling (heating) in those same regions in comparison to a TPV's surroundings. This normally strengthens TPVs when they are isolated from other factors, such as latent heating, and can explain the sometimes-long lifetimes of TPVs. However, too much moisture in the UTLS would counteract this strengthening process, reducing the rate of TPV strengthening in numerical models. If a simulated TPV is too weak, or if TPVs are systematically too weak in climate models, this could in turn impact the strength of extreme weather such as extreme cold air outbreaks, winter storms, and severe thunderstorms.

Recent work has suggested that operational models have deficiencies representing the tropopause structure in the vicinity of the jet stream. Schäfler et al. (2020) used aircraft observations taken during the NAWDEX experiment to assess the European Centre for Medium-Range Weather Forecasts (ECMWF) Integrated Forecasting System (IFS) and the UK Met Office Unified Model. For these flights, the models had a slow-wind bias in the troposphere (and lower stratosphere) of -0.41 m s^{-1} and -0.15 m s^{-1}, respectively, while the median vertical shear at and above the tropopause is underestimated by a factor of 1.5 to 5. Similarly, Lavers et al. (2023) used dropsonde wind and temperature observations collected during the Atmospheric River Reconnaissance (AR Recon) campaign to assess the North Pacific jet stream structure in forecast

models. The results show that the ECMWF IFS has a slow-wind bias of up to -1.88 m s^{-1} on forecast day 4 and cannot resolve the sharp potential vorticity (PV) gradient across the jet stream and tropopause, which becomes worse with time. Consequently, the reduced sharpness of the gradients near the jet would make it difficult for the model to accurately represent tropopause-based waves and downstream forecasts.

4.2. Mesoscale Processes and Dynamics Sampling Strategy

The scientific pursuits of NURTURE aim to systematically sample the mesoscale characteristics of features in regions poleward of the jet stream where conventional in-situ observations are otherwise unable to provide. While TPVs themselves are generally mesoscale, it is the even smaller mesoscale atmospheric features within a TPV that are typically unresolved by conventional observations and models, such as vortex asymmetries, satellite vortex signatures, low-level jets, boundary layer structure, and narrow baroclinic zones that create favorable conditions for the coupling of a TPV with the surface. Similarly, turbulence and mesoscale details that encapsulate the coupling process between upstream features and the larger-scale jet stream are highly desired in jet stream mergers. Mesoscale processes are also of great importance when considering the merger of TPVs with the polar jet stream. In particular, latent heating, radiative processes, turbulence, and ageostrophic secondary circulations within the near-jet environment all play a role in modifying the dynamic tropopause structure during periods in which a TPV merges with the jet. A sampling strategy that bisects the jet in a "lawn mower" pattern along its axis using remote sensors and drop sondes during periods with a TPV merger will illuminate the character and intensity of the aforementioned processes, as well as their degree of spatial heterogeneity. Such characteristics are generally not captured at adequate temporal resolutions (< 3-6 hours) by global forecast datasets and most reanalysis and climate model datasets. For diabatic heating near the jet, the important aspect to measure is how the nearby upper-tropospheric divergent wind is impinging on the jet; therefore, the sampling strategy would involve flying in a circle around the main region of diabatic heating and parallel to the jet, sampling the wind and temperature field using remport sensors and drop sondes.

Observing the lower-tropospheric boundary layer characteristics and processes is an important component of the NURTURE program. Remote sensors and dropsondes will provide the capability to link the upper-tropospheric and lower-stratospheric mesoscale features and circulations such as jet streams and TPVs with lower tropospheric phenomena, such as low-level jets, and boundary layer circulations. The lower tropospheric and boundary layer observing strategy will consist of transects from flight level in the upper- to middle-troposphere, beneath features of interest such as jet streams and TPVs, to characterize the moisture and heat transport via low-level jets, and boundary layer recovery processes in regions of cold-air outbreaks resulting in strong sensible and latent heat fluxes over continental and oceanic. The flight transects can be oriented along low-level jet features and normal to the low-level jet axis. In the cold-air outbreak regions, flight legs oriented along the low-level flow will be utilized to characterize the lower troposphere and boundary layer transport and circulations.

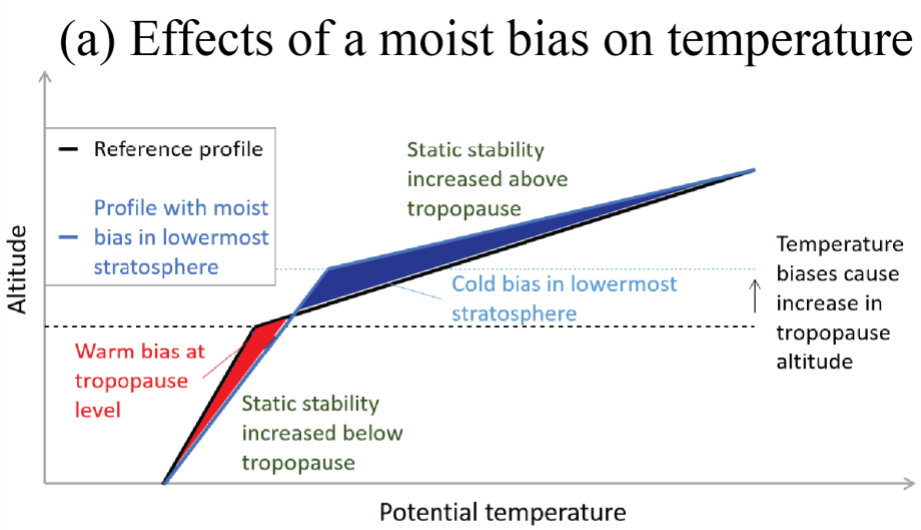

Adapted from Bland et al., 2021

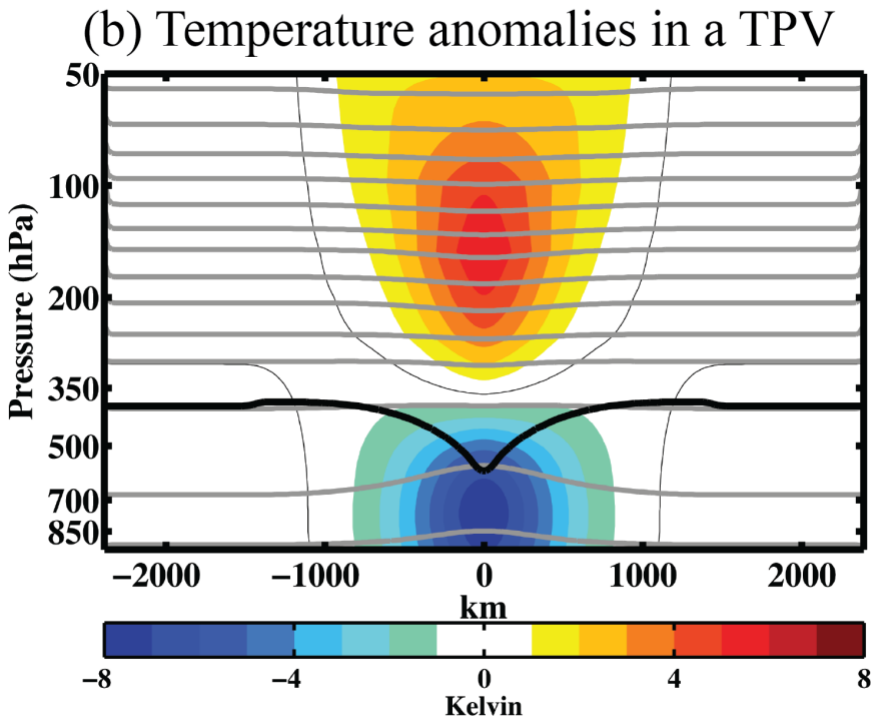

From Cavallo and Hakim, 2013

Figure 6: (a) Schematic illustration of the effect of the lowermost stratospheric moist bias on an idealized vertical profile of potential temperature, where the black line is an idealized reference profile. The blue line represents the profile following the effects of the anomalous radiative heating dipole resulting from a moist bias. The horizontal dotted lines indicate the tropopause altitudes for the respective profiles (from Figure 10 of Bland et al. 2021). (b) Cross-vortex section of potential temperature through an idealized cyclonic tropopause polar vortex (from Figure 2b of Cavallo and Hakim 2013). Colors show anomalies, while contours show the mean field. The thick black contour denotes the dynamic tropopause, represented by the 2-PVU surface. The color interval is 1 K, and the contour interval is 20 K.

4.3 Modeling needs

UTLS uncertainties can result in detrimental impacts in both weather and climate models. As discussed in Section 2.1, numerical weather models have systematic biases in UTLS water vapor and in the representation of the tropopause in the vicinity of jet streams. During the formation and/or evolution of HIW events, numerical weather models can still feature drastic reductions in forecast skill. This is illustrated here in the case of extratropical storm Ciara, which occurred in February 2020. This case will be discussed in further detail in Section 4.3.3, as it had significant impacts in the United States, North Atlantic, and Europe. A strengthening of Ciara occurred as it approached Europe in association with the formation of a "superjet", or region of particularly strong jet stream winds in the North Atlantic on 7 February 2020. The formation of this "superjet" occurred as a result of a superposition between the polar and subtropical jets, as well as a TPV. Numerical weather models struggled to forecast this superposition event, which is apparent in the large decrease in 5-day plus forecast skill for this event (Figure 7).

In numerical climate models, temperature is particularly sensitive to water vapor in the UTLS region, and due to the relatively long radiative time scales in the UTLS, water vapor in this region can have a substantial impact on surface temperatures and global climate (e.g., Forster and Shine 2002; Solomon et al. 2010; Dessler et al. 2013; Wang et al. 2017). Water vapor in the UTLS acts as a positive climate feedback, where increases in water vapor further increase global surface temperatures (Graversen and Wang 2009; Dessler et al. 2013; Nowack et al. 2023). The vertical structure of atmospheric warming leads to negative climate feedback at lower latitudes and positive climate feedback at higher latitudes, depending on how much warming occurs in the upper-troposphere (e.g, Manabe and Wetherald 1975; Bintanja et al. 2012; Pithan and Mauritsen 2014). Furthermore, gradients in radiatively important greenhouse gasses such as ozone and water vapor are very high across the tropopause, and their representation in models depends on an accurate representation of the tropopause structure (e.g., Randel et al. 2007; Gettelman et al. 2011). While the sources of stratospheric water vapor are an active area of research currently, some likely sources include tropopause-overshooting convection and the meridional isentropic transport of air from the tropical upper troposphere to the extratropical lower stratosphere (Tinney and Homeyer 2023). Therefore, additional observations of water vapor in the UTLS are crucial in order to understand these processes better and to alleviate the barriers of using numerical models for such studies.

The predictability of high-impact weather is thought to be closely related to the characteristics of the jet stream and the PV anomalies associated with the Rossby waves propagating along it. A study by Rodwell et al. (2013) revealed a common precursor for the worst 100 poor forecasts or busts over Europe over a decade period of time. Six days prior, a distinctive Rossby wave pattern emerged, featuring a pronounced trough over the Rockies and a downstream ridge transporting warm, moist air from the southern USA to the eastern region. The authors suggested that diabatic processes in mesoscale weather systems over the USA contribute to reduced predictability in these cases, potentially stemming from systematic misrepresentations of the key processes in forecast models that travel along the jet stream. Analogously in higher latitudes, the mesoscale PV anomalies associated with TPVs in the UTLS and related diabatic processes may have a strong influence over the downstream predictability of high-impact weather phenomena. The longwave radiative cooling maximum that occurs just below the tropopause, associated with the rapid change in water vapor may act to reinforce TPVs enhancing local PV maxima (Chagnon et al., 2013, Cavallo and Hakim, 2012), perturbing the jet stream triggering Rossby wave packets that

propagate rapidly downstream. The TPVs and their associated mesoscale PV anomalies and jet streaks can spawn high-impact weather events through baroclinic interactions with the lower troposphere including boundary layer processes. The degree to which the mesoscale characteristics of TPVs influence high-impact weather predictability is relatively unexplored, and observations of the TPVs and their interactions with baroclinic and diabatic processes are needed to address the predictability characteristics.

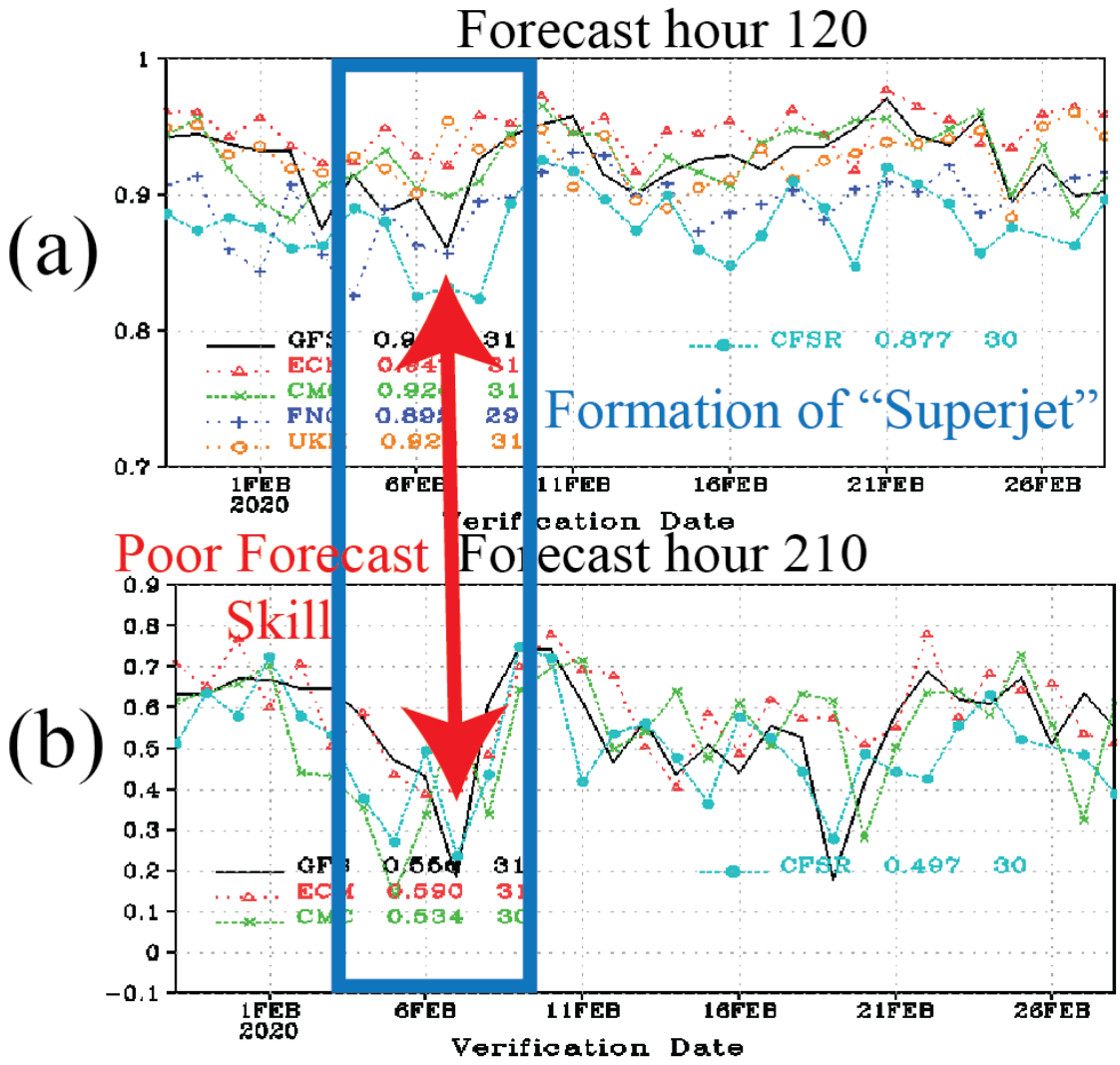

Figure 7: Northern Hemisphere anomaly correlation coefficients (ACCs) at forecast lead times of (a) 120 hours and (b) 210 hours from the GFS (black), ECMWF (red), CMC (green), FNC (blue), and UKMET (orange) global models in February 2020. Lower (higher) ACCs represent relatively poor (good) forecast skill. Skillful forecasts contain ACC values above ~0.6. A "superjet" formed on 7 February 2020, and the period surrounding this time is highlighted in the blue box. The red arrows point to the times of the lowest forecast skill.

5. Experimental Design

5.1. Geophysical measurements needed to address the science questions

In order to address the science questions, NURTURE will utilize the broad capabilities of the NASA 777 aircraft. Table 1 below maps the science questions to specific geophysical variables needed to meet the objectives.

Geophysical Variables	Tropopause Structure and Dynamics		Diabatic Processes	Boundary Layer Processes	
	SQ1.1	SQ1.2	SQ2.1	SQ3.1	SQ3.2
Temperature Profile	x	x		x	x
Humidity Profile	x	x	x	x	x
3-D Winds	x	x		x	x
Ozone (profile)	x	x			
Cloud top Height	x	x	x	x	x
Cloud top phase	x	x	x	x	x
Cloud top temperature	x	x	x	x	x
Cloud depth	x	x	x	x	x
Cloud/Precip profile	x	x	x	x	x
Doppler velocity in cloud for environmental vertical velocity	x	x	x		
Short-wave radiation	x	x	x		
Long-wave radiation	x	x	x		
PBL height				x	x
Turbulence at flight level	x	x			x
SST, surface winds over water				x	x

Table 1: Geophysical variables that need to be observed to address the science questions and hypotheses as listed in Figure 5.

5.2. Sampling Strategy

5.2.1. Deployment location

The NASA 777 is anticipated to have a range of 5500 – 7700 nautical miles (10186 – 14260 km), depending on the exact payload. In determining the location to base operations, the following criteria are considered:

- Airports with runways and facilities that can accommodate a 777 aircraft,
- Locations along the Eastern North American coast so that both the HIW events and their upstream targets are within an optimal range,
- Close proximity to the jet stream to maximize the sampling where the upstream targets are merging into the jet stream and
- Ideally, locations on the poleward side of the jet since the targets focus on perturbations poleward of the jet stream.

Given the above criteria, the base of operations will nominally be Gander, Newfoundland and Labrador, Canada, or a similar location. For the purposes of this discussion below, we will reference Gander as the hypothetical base of operations. Gander International Airport and Canadian Forces Base (CFB) Gander share an airfield that contains two active asphalt runways of length 8900 ft (2713 m) and 10200 ft (3109 m). The airport is equipped to accommodate aircraft such as the 777 and is a common refueling stop for transatlantic aircraft. Gander is also located just poleward of the climatological January-February jet stream, with a range encompassing most of Canada, the continental United States, the North Atlantic, and the western portions of Europe (Figure 8). With this range, we expect upstream targets to be sampled as far as one week before a HIW event. Furthermore, this leaves an opportunity for downstream sampling of the HIW events themselves.

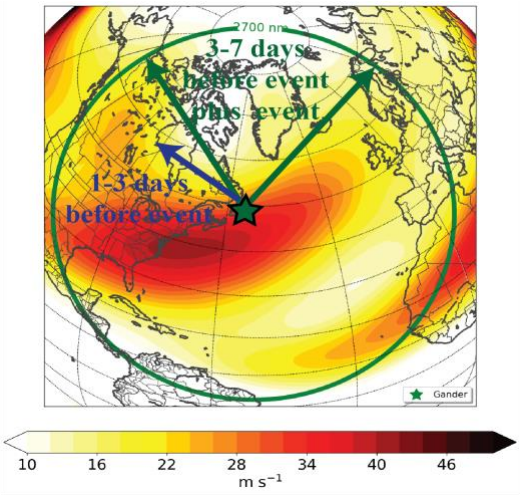

Figure 8: Deployment summary for NURTURE. The approximate range of the NASA 777 aircraft is shown with the green circle for a home base of Gander, Newfoundland and Labrador, Canada. The NASA 777 will be able to sample upstream features 3-5+ days in advance of an event, and will also be within range to sample the resulting downstream high-impact weather events. The colors show the January-February climatological mean wind at 300 hPa from 1991 to 2020.

5.2.2. Climatology

TPVs are mostly generated in the Canadian Archipelago region in far northern Canada (Cavallo and Hakim 2010). Their generation mechanism is not yet very well understood but is likely due to the splitting away from existing TPVs from shear and deformation in the larger-scale atmospheric flow (Bray and Cavallo 2022). The probability that there will be a TPV within about 1˚ latitude of a given point during the winter ranges from over a 40 percent chance per day in the Canadian Archipelago, to around 10-20 percent per

day in southeastern Canada (Figure 9a). Thus, coastal areas of eastern Canada can expect to see one TPV passing directly by roughly every 5-10 days during the winter. While the locations of TPVs mostly stay limited to the Arctic during the summer, their spatial distributions exhibit strong seasonal variability. During the winter, TPVs tend to move out of the Arctic in two primary pathways over northern Canada and eastern Siberia (Figure 9b). The longest-lived TPVs (lifetimes of greater than 2 weeks) are equally likely to exit the Arctic through these pathways during the winter (Bray and Cavallo 2022). In the North American TPV pathway, TPVs generally move equatorward from the Canadian Archipelago region and into southeastern Canada. During the winter, the polar jet stream is stronger and Rossby Waves exhibit more frequent intrusions into the Arctic; thus the larger-scale atmospheric flow more readily advects TPVs out of the Arctic to lower latitudes. The frequency of jet streaks exceeding 100 m s^{-1} greatest at locations where TPVs exiting the Arctic through the North American pathway intersect the jet stream, further supporting the notion that TPVs play an important role in the formation of anomalously strong jet streaks (Figure 9c). While the climatology suggests to expect about 4-8 TPVs in coastal Canada to 14 in northern Canada during the 6-week campaign period, an aircraft campaign could feasibly obtain enough data to meet the mission objectives from two TPVs and one superposition event.

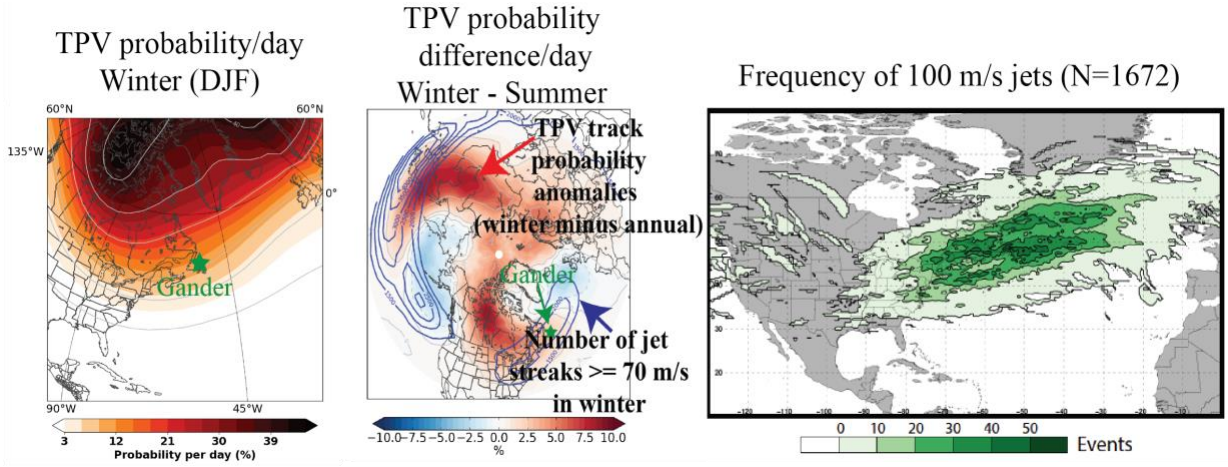

Figure 9: (a) Daily probability of a TPV at any given location during the winter months of December, January, and February (DJF). (b) The difference in the daily probability of a TPV in the winter months (DJF) minus the summer months (June, July, and August; JJA). Blue contours show the number of jet streaks >= 70 m s^{-1} during DJF. Data are from 1979-2019 ERA5. (c) Frequency of 100 m s^{-1} jet stream winds. Data are from ERA-interim from 1981-2010. The location of Gander is denoted with a green star in panels (a) and (b).

5.2.3. Example missions

To further elucidate the sampling strategies for this campaign, examples of hypothetical deployments using past HIW events that occurred in January-February will now be discussed. One event was the strongest Arctic Cyclone on record with a minimum sea-level pressure reaching 932 hPa on 24 January 2022 in the North Atlantic near Svalbard, Norway (Blanchard-Wrigglesworth et al. 2022). Associated with this HIW event were record 1-hour wind speeds, reaching over 28 m s^{-1} on 24 January over the Barents Sea. These were the region's strongest wind speeds from 1979-2022. Perhaps most notable was the remarkable loss of sea ice, with a reduction of over 0.4 million km^2 in the Kara and Barents Seas in just a 7-day period (Figure 10). Satellite altimetry indicated that the surface winds generated ocean waves in the Barents Sea that penetrated over 100 km into the sea ice pack with wave heights of up to 2 meters,

leading to the rapid breakup of the sea ice. Soon thereafter, on 28 January, extratropical storm Malik formed in northern Europe, leading to seven fatalities, nearly 3,000 severe wind reports, and over 800,000 power outages in multiple countries, costing a total of $415 million U.S. Dollars in damages.

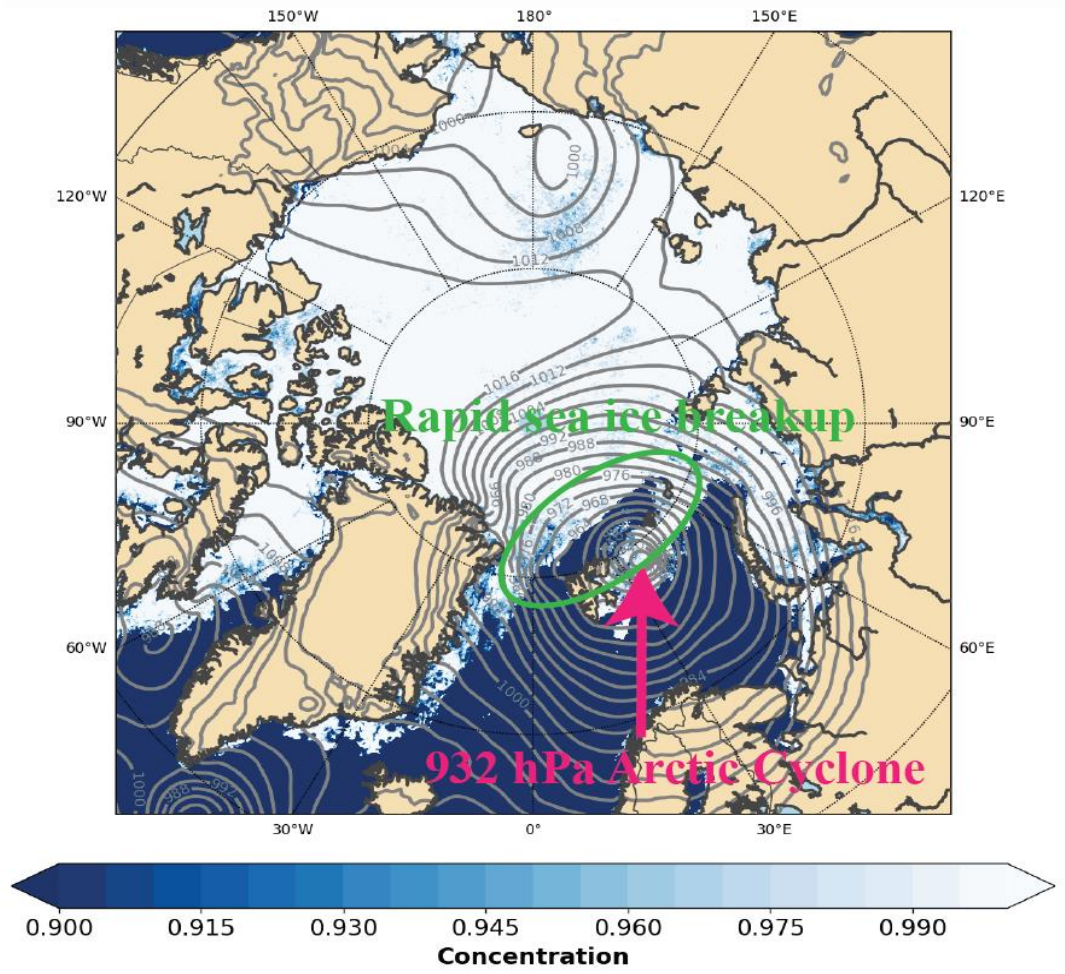

Figure 10: Sea ice concentrations (colors) from passive microwave satellite radiometry composited over 24 January 2022. The green circle highlights a locally reduced sea ice concentration region under an observationally based Arctic Cyclone reanalysis. Gray contours are mean sea level pressure from the ERA5.

The primary TPV that led to the record strength of the Arctic Cyclone entered the range of Gander around 11 January 2022. This primary TPV drifted around the Canadian Archipelago for the next week, and by 17 January (one week before this HIW event) it was located over Hudson Bay (Figures 11a,d). A sample flight mission would be to transect the TPV from two different directions and sample the nearby smaller satellite TPVs that could potentially influence the larger parent TPV at later times. Meanwhile, three days before the HIW, the Arctic Cyclone is beginning to form in association with a different, smaller TPV that developed in the Canadian Archipelago on 16 January. One flight mission could be to sample both the downstream developing Arctic Cyclone and the upstream TPVs that became important for the additional intensification of the Arctic Cyclone (Figures 11b,e). Also, the primary TPV began to approach the polar jet stream three days before the event. At this stage, missions could also focus on the merger of

the parent TPV with the polar jet stream, occurring almost directly over Gander. The fine temporal details of such a merging process have never been directly observed. On the day of the event, missions could focus on observing the record-breaking Arctic Cyclone and the rapid sea ice breakup (Figures 11c,f). Rapid sea ice breakups have only been previously observed by satellite measurements.

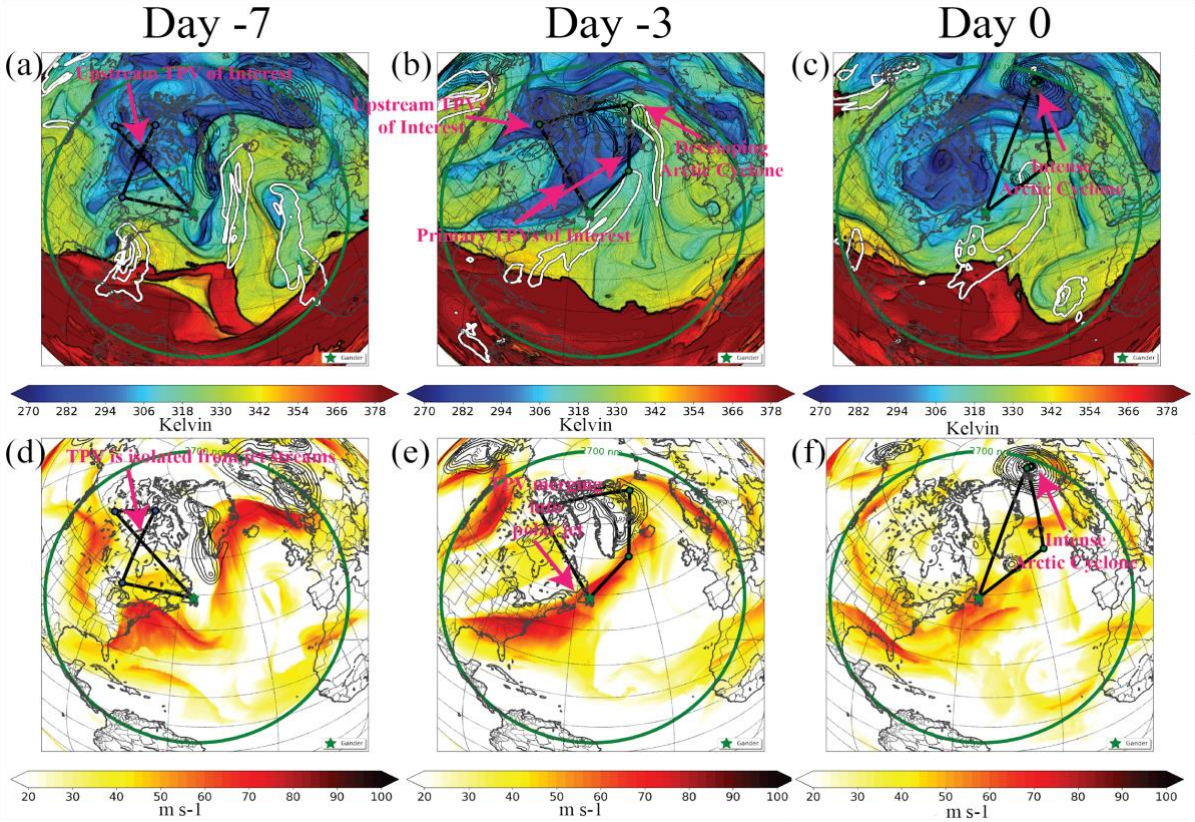

Figure 11: Hypothetical NASA 777 (thick black) flight tracks with (a)-(c) potential temperature and (d)-(e) wind (a),(d) 7 days, (b),(e) 1 day, and (c), (f) 0 days before a high impact weather event on the dynamic tropopause (colors; the color interval is 1 K in (a)-(c) and 1 m s^{-1} in (d)-(f)) and sea level pressure (black contours; contour interval 4 hPa; only values at or below 1004 hPa are shown). The dynamic tropopause is the 2 PVU surface, where 1 PVU = 10^6 K m^2 kg^{-1} s^{-1}. Data are from ERA5 valid at (a), (d) 17 January at 00 UTC, (b), (e) 21 January at 12 UTC, and (c),(f) 24 January at 12 UTC 2022. The green circles indicate the range of the NASA 777.

A second strategic deployment example is highlighted by sampling the upstream precursors to the HIW events associated with extratropical storm Ciara in February 2020. Ciara formed in the Southern Great Plains of the United States on 3 February 2020 and tracked across the northeastern United States, Canadian Maritimes, and North Atlantic, ultimately strengthening to a 922 hPa cyclone in Europe before decaying on 16 February off the coast of Finland. Ciara's rapid intensification as it approached Europe was associated with a TPV that merged into the polar jet stream, creating a "superjet" in the North Atlantic on 8-9 February with wind speeds exceeding 100 m s^{-1} (over 220 mph). Concurrent with the merger of the TPV with the polar jet stream, there was a Northern Hemisphere forecast dropout, where 5+ day forecast skills dropped substantially (Recall Figure 7). Furthermore, a stratospheric wave reflection and downward stratosphere-troposphere coupling event occurred during the first ten days of February. For the purposes of sampling this event, the day of the event will be defined as the day that storm Ciara began to impact

Europe on 9 February 2020. Five days before the event, Ciara had already formed in the southern United States. At the same time, a mature cyclone near Gander with several upstream TPVs were observed. These features became important for Ciara's continued development once it arrived in the Northern Atlantic (Figures 12a,d). Thus, missions could focus on sampling the nearby cyclone as well as the upstream TPVs. Two days before the event, it becomes clear that there is a primary TPV moving directly toward the polar jet stream (Figures 12b,e). The merging of the TPV into the jet stream takes place over about two days, in extremely close range to Gander, providing ample sampling opportunities (Figures 12c,f). During these missions, some of the additional observations from the 777 could likely have been included in operational model data assimilation updates, potentially improving the forecast skill. From 9 – 11 February 2020, storm Ciara strengthened to a 920 hPa cyclone in Europe, resulting in 17 fatalities, around 1.2 million power outages, and over $2 billion U.S. Dollars in damages.

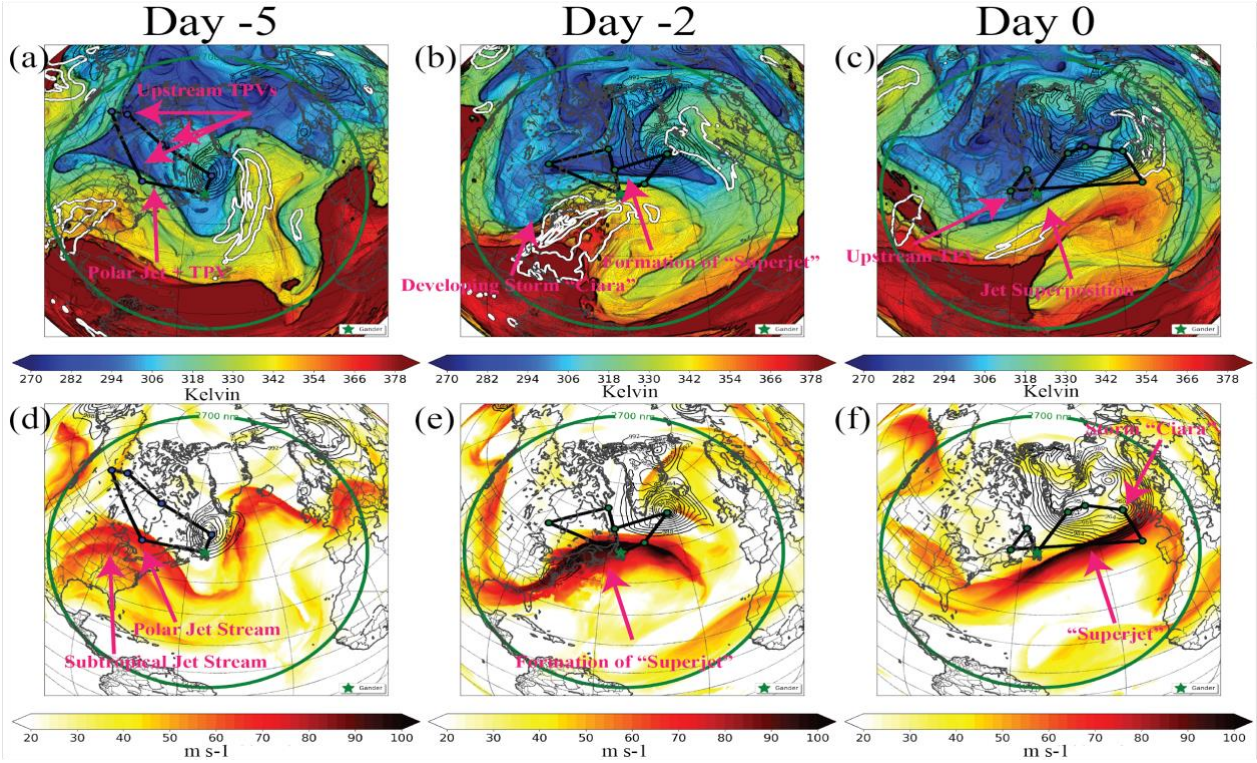

Figure 12: Hypothetical NASA 777 (thick black) flight tracks (a)-(c) potential temperature and (d)-(e) wind (a),(d) 5 days, (b),(e) 2 days, and (c), (f) 0 days before a high impact weather event on the dynamic tropopause (colors; color interval is 1 K in (a)-(c) and 1 m s^{-1} in (d)-(f)) and sea level pressure (black contours; contour interval 4 hPa; only values at or below 1004 hPa are shown). The dynamic tropopause is the 2 PVU surface, where 1 PVU = 10^6 K m^2 kg^{-1} s^{-1}. Data are from ERA5 valid at (a), (d) 04 February at 00 UTC, (b), (e) 07 February at 12 UTC, and (c),(f) 09 February at 06 UTC 2020. The green circles indicate the range of the NASA 777.

6. References

Ahmadi-Givi, F., G. C. Craig, and R. S. Plant, 2004: The dynamics of a midlatitude cyclone with very strong latent-heat release. *Quart. J. Roy. Meteor. Soc.*, **130**, 295–323, doi: 10.1256/qj.02.226.

Archambault, H. M., L. F. Bosart, D. Keyser, and J. M. Cordeira, 2013: A climatological analysis of the extratropical flow response to recurving western North Pacific tropical cyclones. *Mon. Wea. Rev.*, **141**, 2325–2346, doi: 10.1175/MWR-D-12-00257.1.

Archambault, H. M., D. Keyser, L. F. Bosart, C. A. Davis, and J. M. Cordeira, 2015: A composite perspective of the extratropical flow response to recurving western North Pacific tropical cyclones. *Mon. Wea. Rev.*, **143**, 1122–1141, doi: 10.1175/MWR-D-14-00270.1.

Attard, H. E., and Lang, A. L. 2019: The Impact of Tropospheric and Stratospheric Tropical Variability on the Location, Frequency, and Duration of Cool-Season Extratropical Synoptic Events. *Mon. Wea. Rev.*, **147**, 519–542. doi: 10.1175/MWR-D-18-0039.1

Barnhart, K. R., C. R. Miller, I. Overeem, and J. E. Kay, 2016: Mapping the future expansion of Arctic open water. *Nature Climate Change*, **6**, 280–285.

Baumgart, M., M. Riemer, V. Wirth, F. Teubler, and S. T. K. Lang, 2018: Potential vorticity dynamics of forecast errors: A quantitative case study. *Mon. Wea. Rev.*, **146**, 1405–1425, doi: 10.1175/MWR-D-17-0196.1.

Baumgart, M., P. Ghinassi, V. Wirth, T. Selz, G. C. Craig, and M. Riemer, 2019: Quantitative view on the processes governing the upscale error growth up to the planetary scale using a stochastic convection scheme. *Mon. Wea. Rev.*, **147**, 1713–1731.

Bentley, A. M., L. F. Bosart, and D. Keyser, 2019: A climatology of extratropical cyclones leading to extreme weather events over central and eastern North America. *Mon. Wea. Rev.*, **147**, 1471–1490, doi: 10.1175/MWR-D-18-0453.1.

Berman, J.D., and R. D. Torn, 2019: The impact of initial condition and warm conveyor belt forecast uncertainty on variability in the downstream waveguide in an ECMWF case study. *Mon. Wea. Rev.*, **147**, 4071–4089, doi: 10.1175/MWR-D-18-0333.1.

Berman, J. D., and R. D. Torn 2022: The Sensitivity of Downstream Waveguide Forecasts to Upstream Warm Conveyor Belt Forecast Uncertainty using MPAS. *Mon. Wea. Rev.*, **150**, 2573–2592

Biernat, K. A., L. F. Bosart, and D. Keyser, 2021: A climatological analysis of the linkages between tropopause polar vortices, cold pools, and cold air outbreaks over the central and eastern U.S. *Mon. Wea. Rev.*, **149,** 189–206, doi: 10.1175/MWR-D-20-0191.1.

Bintanja, R., E. Van der Linden, and W. Hazeleger, 2012: Boundary layer stability and Arctic climate change: A feedback study using EC-Earth. *Climate Dynamics*, **39**, 2659–2673.

Blanchard-Wrigglesworth, E., M. Webster, L. Boisvert, C. Parker, and C. Horvat, 2022: Record Arctic cyclone of January 2022: Characteristics, impacts, and predictability. *Journal of Geophysical Research: Atmospheres*, e2022JD037161.

Bland, J., S. Gray, J. Methven, and R. Forbes, 2021: Characterising extratropical near-tropopause analysis humidity biases and their radiative effects on temperature forecasts. *Quart. J. Roy. Meteor. Soc.*, **147**, 3878–3898, doi: 10.1002/qj.4150.

Boljka, L., and T. Birner, 2022: Potential impact of tropopause sharpness on the structure and strength of the general circulation. *Npj Clim. Atmos. Dyn.*, **5**, Article 1. doi: 10.1038/s41612-022-00319-6

Borg, S. M., S. M. Cavallo, and D. D. Turner, 2020: Characteristics of Tropopause Polar Vortices Based on Observations over the Greenland Ice Sheet. *Journal of Applied Meteorology and Climatology*, **59**, 1933–1947.

Bosart, L. F., G. J. Hakim, K. R. Tyle, M. A. Bedrick, W. E. Bracken, M. J. Dickinson, and D. M. Schultz, 1996: Large-scale antecedent conditions associated with the 12–14 March 1993 cyclone ("superstorm '93") over eastern North America. *Mon. Wea. Rev.*, **124**, 1865–1891, doi: 10.1175/1520-0493(1996)124<1865:LSACAW>2.0.CO;2.

Bosart, L. F., B. J. Moore, J. M. Cordeira, and H. M. Archambault, 2017: Interactions of North Pacific tropical, midlatitude, and polar disturbances resulting in linked extreme weather events over North America in October 2007. *Mon. Wea. Rev.*, **145**, 1245–1273, doi: 10.1175/MWR-D-16-0230.1.

Bray, M., S. M. Cavallo, and H. Bluestein, 2021: Examining the relationship between tropopause polar vortices and severe weather outbreaks. *Weather and Forecasting*, **36**, 1799–1814.

Bray, M. T., and S. M. Cavallo, 2022: Characteristics of long-track tropopause polar vortices. *Weather and Climate Dynamics*, 1–36.

Browning, K. A., 1971: Radar measurements of air motion near fronts. *Weather*, **26**, 320–340.

Butler, A., A. Charlton-Perez, D. I. V. Domeisen, C. Garfinkel, E. P. Gerber, P. Hitchcock, A. Karpechko, A. C. Maycock, M. Sigmond, I. Simpson, and S.-W. Son, 2019: Chapter 11—Sub-seasonal Predictability and the Stratosphere. In A. W. Robertson and F. Vitart (Eds.), *Sub-Seasonal to Seasonal Prediction* pp. 223–241: Elsevier. doi: 10.1016/B978-0-12-811714-9.00011-5

Byers, H., H. Landsberg, H. Wexler, B. Haurwitz, A. Spilhaus, H. Willett, and H. Houghton, 1951: Anticyclones. *Compendium of Meteorology*, Springer, 621–629.

Carlson, T. N., 1980: Airflow through midlatitude cyclones and the comma cloud pattern. *Mon. Wea. Rev.*, **108**, 1498–1509.

Cavallo, S. M., and G. J. Hakim, 2009: Potential vorticity diagnosis of a tropopause polar cyclone. *Mon. Wea. Rev.*, **137**, 1358–1371.

——, and ——, 2012: Radiative impact on tropopause polar vortices over the Arctic. *Mon. Wea. Rev.*, **140**, 1683–1702.

——, and ——, 2013: The physical mechanisms of tropopause polar cyclone intensity change. *J. Atmos. Sci.*, **70**, 3359–3373.

——, J. Berner, and C. Snyder, 2016: Diagnosing model error from time–averaged tendencies in the Weather Research and Forecasting model. *Mon. Wea. Rev.*, **144**, 759–779.

Cellitti, M. P., J. E. Walsh, R. M. Rauber, and D. H. Portis, 2006: Extreme cold air outbreaks over the United States, the polar vortex, and the large-scale circulation. *J. Geophys. Res.*, **111**, D02114, doi: 10.1029/2005JD006273.

Chang, E. K. M., S. Lee, and K. L. Swanson, 2002: Storm track dynamics. *J. Climate*, **15**, 2163–2183, doi: 10.1175/1520-0442(2002)015<02163:STD>2.0.CO;2.

Charlton-Perez, A. J., L. Ferranti, and R. W. Lee, 2018: The influence of the stratospheric state on North Atlantic weather regimes. *Quart. J. Roy. Meteor. Soc*., 144(713), 1140–1151. doi: 10.1002/qj.3280

Christenson, C. E., J. E. Martin, Z. J. Handlos, 2017: A synoptic climatology of Northern Hemisphere, cold season polar and subtropical jet superposition events. *J. Climate*, **30**, 7231–7246, doi: 10.1175/JCLI-D-16-0565.1.

Colle, B. A., and C. F. Mass, 1995: The structure and evolution of cold surges east of the Rocky Mountains. *Mon. Wea. Rev.*, **123**, 2577–2610, doi: 10.1175/1520-0493(1995)123<2577:TSAEOC>2.0.CO;2.

Curry, J. A., 1983: On the formation of continental polar air. *Journal of the Atmospheric Sciences*, **40**, 2278–2292.

——, 1987: The contribution of radiative cooling to the formation of cold-core anticyclones. *Journal of the Atmospheric Sciences*, **44**, 2575–2592.

Dacre, H. F., P. A. Clark, O. Martinez-Alvarado, M. A. Stringer, and D. A. Lavers, 2015: How do atmospheric rivers form? *Bull. Amer. Meteor. Soc.*, **96**, 1243–1255, doi: 10.1175/BAMS-D-14-00031.1.

Davis, C. A., M. Stoelinga, and Y. Kuo, 1993: The integrated effect of condensation in numerical simulations of extratropical cyclogenesis. *Mon. Wea. Rev.*, **121**, 2309–2330.

Dessler, A., M. Schoeberl, T. Wang, S. Davis, and K. Rosenlof, 2013: Stratospheric water vapor feedback. *Proceedings of the National Academy of Sciences*, **110**, 18087–18091.

Dole, R., M. Hoerling, A. Kumar, J. Eischeid, J. Perlwitz, X.-W. Quan, G. Kiladis, R. Webb, D. Murray, M. Chen, K. Wolter, and T. Zhang, 2014: The making of an extreme event: Putting the pieces together. *Bull. Amer. Meteor. Soc.*, **95**, 427– 440, doi: 10.1175/BAMS-D-12-00069.1.

Domeisen, D., A. Butler, A. Charlton-Perez, B. Ayarzagüena, M. Baldwin, E. Dunn-Sigouin, J. Furtado, C. Garfinkel, P. Hitchcock A. Karpechko, H. Kim, J. Knight, A. L. Lang, E.-P. Lim, A. Marshall, G. Roff, C. Schwartz, I. Simpson, S.-W. Son, M. Taguchi. 2020: The Role of the Stratosphere in Subseasonal to Seasonal Prediction: 2. Predictability Arising From Stratosphere-Troposphere Coupling. *J. Geophys. Res: Atmos*., 125(2), e2019JD030923. doi: 10.1029/2019JD030923

Dyroff, C., A. Zahn, E. Christner, R. Forbes, A. M. Tompkins, and P. F. van Velthoven, 2015: Comparison of ECMWF analysis and forecast humidity data with CARIBIC upper troposphere and lower stratosphere observations. *Quarterly Journal of the Royal Meteorological Society*, **141**, 833–844.

Fang, Z., P. T. Freeman, C. B. Field, and K. J. Mach, 2018: Reduced sea ice protection period increases storm exposure in Kivalina, Alaska. *Arctic Science*, **4**, 525–537, https://doi.org/10.1139/as-2017-0024.

Feist, D., A. Geer, S. Müller, and N. Kämpfer, 2007: Middle atmosphere water vapour and dynamical features in aircraft measurements and ECMWF analyses. *Atmospheric chemistry and physics*, **7**, 5291–5307.

Forster, P. M. de F., and K. Shine, 2002: Assessing the climate impact of trends in stratospheric water vapor. *Geophysical Research Letters*, **29**.

Fröhlich, L., P. Knippertz, A. H. Fink, and E. Hohberger, 2013: An objective climatology of tropical plumes. *J. Climate*, **26**, 5044–5060, doi: 10.1175/JCLI-D-12-00351.1.

Gettelman, A., P. Hoor, L. Pan, W. Randel, M. I. Hegglin, and T. Birner, 2011: The extratropical upper troposphere and lower stratosphere. *Reviews of Geophysics*, **49**, https://doi.org/10.1029/2011RG000355.

Gordon, A. E., S. M. Cavallo, and A. K. Novak, 2023: Evaluating Common Characteristics of Antarctic Tropopause Polar Vortices. *J. of the Atmos. Sci.*, **80**, 337–352, https://doi.org/10.1175/JAS-D-22-0091.1.

Grams, C. M., H. Wernli, M. Böttcher, J. Čampa, U. Corsmeier, S. C. Jones, J. H. Keller, C.-J. Lenz, and L. Wiegand, 2011: The key role of diabatic processes in modifying the upper- tropospheric wave guide: A North Atlantic case-study. *Quart. J. Roy. Meteor. Soc.*, **137,** 2174–2193, doi: 10.1002/qj.891.

Grams, C., L. Magnusson, and E. Madonna, 2018: An atmospheric dynamics perspective on the amplification and propagation of forecast error in numerical weather prediction models: A case study. *Quart. J. Roy. Meteor. Soc.*, **144**, 2577–2591.

Graversen, R. G., and M. Wang, 2009: Polar amplification in a coupled climate model with locked albedo. *Climate Dynamics*, **33**, 629–643.

Gray, S. L., C. M. Dunning, J. Methven, G. Masato, and J. M. Chagnon, 2014: Systematic model forecast error in Rossby wave structure. *Geophys. Res. Lett.*, 41, 2979–2987, doi: 10.1002/2014GL059282.

Gray, S. L., K. I. Hodges, J. L. Vautrey, and J. Methven, 2021: The role of tropopause polar vortices in the intensification of summer Arctic cyclones. *Wea. Clim. Dyn.*, **2**, 1303–1324. doi: 10.5194/wcd-2-1303-2021

Green, J. S. A., F. H. Ludlam, and J. F. R. McIlven, 1966: Isentropic relative-flow analysis and the parcel theory. *Quart. J. Roy. Meteor. Soc.*, **92**, 210–219

Grotjahn, R., and R. Zhang, 2017: Synoptic analysis of cold air outbreaks over the California Central Valley. *J. Climate*, **30**, 9417–9433, doi: 10.1175/JCLI-D-17-0167.1.

Gu, L., P. J. Hanson, W. Mac Post, D. P. Kaiser, B. Yang, R. Nemani, S. G. Pallardy, and T. Meyers, 2008: The 2007 eastern US spring freeze: Increased cold damage in a warming world? *BioScience*, **58**, 253–262, doi: 10.1641/B580311.

Hakim, G. J., 2000: Climatology of coherent structures on the extratropical tropopause. *Monthly Weather Review*, **128**, 385–406, https://doi.org/10.1175/1520-0493(2000)128<0385:COCSOT>2.0.CO;2.

——, and A. K. Canavan, 2005: Observed cyclone-anticyclone tropopause asymmetries. *Journal of the Atmospheric Sciences*, **62**, 231–240.

Hakim, G. J., L. F. Bosart, and D. Keyser, 1995: The Ohio Valley wave-merger cyclogenesis event of 25–26 January 1978. Part I: Multiscale case study. *Monthly Weather Review*, **123**, 2663– 2692, doi: 10.1175/1520-0493(1995)123<2663:TOVWMC>2.0.CO;2.

Handlos, Z. J., and J. E. Martin, 2016: Composite analysis of large-scale environments conducive to west Pacific polar/subtropical jet superposition. *J. Climate*, **29**, 7145–7165, doi: 10.1175/JCLI-D-16-0044.1.

Handlos, Z. J., and J. E. Martin, 2021: Composite life cycle of west Pacific jet-superposition events and the large-scale environmental response over western North America. *Mon. Wea. Rev.*, **149**, 1105–1124, doi: 10.1175/MWR-D-20-0130.1.

Hardiman, S. C., and Coauthors, 2015: Processes controlling tropical tropopause temperature and stratospheric water vapor in climate models. *Journal of Climate*, **28**, 6516–6535.

Harrold, T. W., 1973: Mechanisms influencing the distribution of precipitation within baroclinic disturbances. *Quart. J. Roy. Meteor. Soc.*, **99**, 232–251.

Harvey, B., J. Methven, C. Sanchez, and A. Schäfler, 2020: Diabatic generation of negative potential vorticity and its impact on the North Atlantic jet stream. *Quart. J. Roy. Meteor. Soc*., **146**, 1477–1497. doi: 10.1002/qj.3747

Hoerling, M., A. Kumar, R. Dole, J. W. Nielsen-Gammon, J. Eischeid, J. Perlwitz, X.-W. Quan, T. Zhang, P. Pegion, and M. Chen, 2013: Anatomy of an extreme event. *J. Climate*, **26**, 2811–2832, doi: 10.1175/JCLI-D-12-00270.1.

Hoskins, B. J., M. E. McIntyre, and A. W. Robertson, 1985: On the use and significance of isentropic potential vorticity maps. *Quarterly Journal of the Royal Meteorological Society*, **111**, 877–946.

Hoskins, B. J., and T. Ambrizzi, 1993: Rossby wave propagation on a realistic longitudinally varying flow. *J. Atmos. Sci.*, **50**, 1661–1671.

Huang, J., P. Hitchcock, A. C. Maycock, and C. M. McKenna, 2021: Northern hemisphere cold air outbreaks are more likely to be severe during weak polar vortex conditions. *Communications Earth & Environment*, **2**, 147.

Ingleby, B., 2017: *An assessment of different radiosonde types 2015/2016*. ECMWF, https://www.ecmwf.int/sites/default/files/elibrary/2017/17551-assessment-different-radiosonde-types-20152016.pdf.

Iskenderian, H., 1995: A 10-year climatology of Northern Hemisphere tropical cloud plumes and their composite flow patterns. *J. Climate*, **8**, 1630–1637, doi: 10.1175/1520-0442(1995)008<1630:AYCONH>2.0.CO;2.

Joos, H., and H. Wernli, 2012: Influence of microphysical processes on the potential vorticity development in a warm conveyor belt: A case-study with the limited-area model COSMO. *Quart. J. Roy. Meteor. Soc.*, **138**, 407–418.

Joos, H. and R. M. Forbes, 2016: Impact of different IFS microphysics on a warm conveyor belt and the downstream flow evolution. *Quart. J. Roy. Meteor. Soc*., **142**, 2727–2739, doi: 10.1002/qj.2863.

Keyser, D., and M. A. Shapiro, 1986: A review of the structure and dynamics of upper-level frontal zones. *Mon. Wea. Rev.*, **114**, 452–499, doi: 10.1175/1520-0493(1986)114<0452:AROTSA>2.0.CO;2.

Klinker, E., and P. D. Sardeshmukh, 1992: The diagnosis of mechanical dissipation in the atmosphere from large-scale balance requirements. *J. Atmos. Sci.*, **49**, 608–627.

Kunz, A., N. Spelten, P. Konopka, R. Müller, R. M. Forbes, and H. Wernli, 2014: Comparison of Fast In situ Stratospheric Hygrometer (FISH) measurements of water vapor in the upper troposphere and lower stratosphere (UTLS) with ECMWF (re) analysis data. *Atmospheric chemistry and physics*, **14**, 10803–10822.

Lavers, D.A., Torn, R.D., Davis, C., Richardson, D.S., Ralph, F.M. & Pappenberger, F.(2023) Forecast evaluation of the North Pacific jet stream using AR Recon dropwindsondes. *Quart. J. Roy. Meteor. Soc*., **149**, 3044–3063, doi: 10.1002/qj.4545.

Lehmann, J., and D. Coumou, 2015: The influence of mid-latitude storm tracks on hot, cold, dry and wet extremes. *Scientific Reports*, **5**, 17491, doi: 10.1038/srep17491.

Li, X., and A. H. Lynch, 2023: New insights into projected Arctic sea road: operational risks, economic values, and policy implications. *Climatic Change*, **176**, 30, https://doi.org/10.1007/s10584-023-03505-4.

Lillo, S. P., S. M. Cavallo, D. B. Parsons, and C. Riedel, 2021: The role of a tropopause polar vortex in the generation of the January 2019 extreme Arctic outbreak. *Journal of the Atmospheric Sciences*, **78**, 2801–2821, https://doi.org/10.1175/JAS-D-20-0285.1.

Manabe, S., and R. T. Wetherald, 1975: The effects of doubling the CO2 concentration on the climate of a General Circulation Model. *J. Atmos. Sci.*, **32**, 3–15.

Martınez-Alvarado, O., E. Madonna, S. Gray, and H. Joos, 2016: A route to systematic error in forecasts of Rossby waves. *Quart. J. Roy. Meteor. Soc.*, **142**, 196–210.

Martius, O., L. M. Polvani, and H. C. Davies, 2009: Blocking precursors to stratospheric sudden warming events. *Geophys.l Res. Lett*, **36**. doi: 10.1029/2009GL038776

Martius, O., C. Schwierz, and H. C. Davies, 2010: Tropopause-level waveguides. *J. Atmos. Sci.*, **67**, 866–879.

Matthias, V., and Kretschmer, M. 2020: The Influence of Stratospheric Wave Reflection on North American Cold Spells. *Mon. Wea. Rev.*, 148(4), 1675–1690. doi: 10.1175/MWR-D-19-0339.1

Miloshevich, L. M., H. Vömel, D. N. Whiteman, B. M. Lesht, F. J. Schmidlin, and F. Russo, 2006: Absolute accuracy of water vapor measurements from six operational radiosonde types launched during AWEX-G and implications for AIRS validation. *J. Geophys. Res.*, **111**, D09S10, https://doi.org/10.1029/2005JD006083.

Moore, B. J., K. M. Mahoney, E. M. Sukovich, R. Cifelli, and T. M. Hamill, 2015: Climatology and environmental characteristics of extreme precipitation events in the southeastern United States. *Mon. Wea. Rev.*, **143**, 718–741, doi: 10.1175/MWR-D-14-00065.1.

Moore, B. J., D. Keyser, and L. F. Bosart, 2019: Linkages between extreme precipitation events in the central and eastern U.S. and Rossby wave breaking. *Mon. Wea. Rev.*, **147**, 3327– 3349, doi: 10.1175/MWR-D-19-0047.1.

Moore, B. J., A. B. White, D. J. Gottas, and P. J. Neiman, 2020: Extreme precipitation events in northern California during winter 2016–17: Multiscale analysis and climatological perspective. *Mon. Wea. Rev.*, **148**, 1049–1074, doi: 10.1175/MWR-D-19-0242.1.

Morgan, M. C., and J. W. Nielsen-Gammon, 1998: Using tropopause maps to diagnose midlatitude weather systems. *Mon. Wea. Rev.*, **126**, 2555–2579, doi: 10.1175/1520-0493(1998)126<2555:UTMTDM>2.0.CO;2.

Mudryk, L. R., J. Dawson, S. E. Howell, C. Derksen, T. A. Zagon, and M. Brady, 2021: Impact of 1, 2 and 4 C of global warming on ship navigation in the Canadian Arctic. *Nature Climate Change*, **11**, 673–679, https://doi.org/10.1038/s41558-021-01087-6.

NOAA, 2021: NOAA National Centers for Environmental Information (NCEI) US billion-dollar weather and climate disasters. https://doi.org/10.25921/stkw-7w73.

Namias, J., and P. F. Clapp, 1949: Confluence theory of the high tropospheric jet stream. *J. Meteor.*, **6**, 330–336, doi: 10.1175/1520-0469(1949)006<0330:CTOTHT>2.0.CO;2.

NCEI, 2023: Billion-dollar weather and climate disasters: Overview, accessed 14 November 2023, https://www.ncdc.noaa.gov/billions/.

Nowack, P., and Coauthors, 2023: Response of stratospheric water vapour to warming constrained by satellite observations. *Nature Geoscience*, 1–7.

Oertel, A., M. Boettcher, H. Joos, M. Sprenger, and H. Wernli, 2020: Potential vorticity structure of embedded convection in a warm conveyor belt and its relevance for large-scale dynamics, *Weather Clim. Dyn.*, **1**, 127–153, doi: 10.5194/wcd-1-127-2020.

Oh, J., and Coauthors, 2018: Ozone sensitivity of tropical upper-troposphere and stratosphere temperature in the MetOffice Unified Model. *Quarterly Journal of the Royal Meteorological Society*, **144**, 2001–2009.

Oikonomou, E., and A. O'Neill, 2006: Evaluation of ozone and water vapor fields from the ECMWF reanalysis ERA-40 during 1991–1999 in comparison with UARS satellite and MOZAIC aircraft observations. *Journal of Geophysical Research: Atmospheres*, **111**.

Palmén, E., and C. W. Newton, 1969: *Atmospheric Circulation Systems: Their Structure and Physical Interpretation*. Academic Press, 603 pp.

Papritz, L., E. Rouges, F. Aemisegger, and H. Wernli, 2019: On the thermodynamic pre-conditioning of Arctic air masses and the role of tropopause polar vortices for cold air outbreaks from Fram Strait. *Journal of Geophysical Research: Atmospheres*, **124**, 11033–11050.

Peterson, T. C., M. P. Hoerling, P. A. Stott, and S. C. Herring, 2013: Explaining extreme events of 2012 from a climate perspective. *Bull. Amer. Meteor. Soc.*, **94**, S1–S74, doi: 10.1175/BAMS-D-13-00085.1.

Pithan, F., and T. Mauritsen, 2014: Arctic amplification dominated by temperature feedbacks in contemporary climate models. *Nature Geoscience*, **7**, 181–184.

Pohorsky, R., M. Röthlisberger, C. M. Grams, J. Riboldi, and O. Martius, 2019: The climatological impact of recurving North Atlantic tropical cyclones on downstream extreme precipitation events. *Mon. Wea. Rev.*, **147**, 1513–1532, doi: 10.1175/MWR-D-18-0195.1.

Pope, V., J. Pamment, D. Jackson, and A. Slingo, 2001: The representation of water vapor and its dependence on vertical resolution in the Hadley Centre Climate Model. *Journal of climate*, **14**, 3065–3085.

Pyle, M. E., D. Keyser, and L. F. Bosart, 2004: A diagnostic study of jet streaks: Kinematic signatures and relationship to coherent tropopause disturbances. *Mon. Wea. Rev.*, **132**, 297–319, https://doi.org/10.1175/1520-0493(2004)132<0297:ADSOJS>2.0.CO;2.

Qu, Z., Y. Huang, P. A. Vaillancourt, J. N. S. Cole, J. A. Milbrandt, M.-K. Yau, K. Walker, and J. de Grandpré, 2020: Simulation of convective moistening of the extratropical lower stratosphere using a numerical weather prediction model. *Atmos. Chem. Phys.*, **20**, 2143–2159, doi: 10.5194/acp-20-2143-2020.

Quinting, J., and S. C. Jones, 2016: On the impact of tropical cyclones on Rossby wave packets: A climatological perspective. *Mon. Wea. Rev.*, **144**, 2021–2048.

Ralph, F. M., P. J. Neiman, G. A. Wick, S. I. Gutman, M. D. Dettinger, D. R. Cayan, and A. B. White, 2006: Flooding on California's Russian River: Role of atmospheric rivers. *Geophys. Res. Lett.*, **33**, L13801, doi: 10.1029/2006GL026689.

Randel, W. J., F. Wu, and P. Forster, 2007: The extratropical inversion layer: Global observations with GPS data, and a radiative forcing mechanism. *J. Atmos. Sci.*, **64**, 4489–4496, https://doi.org/10.1175/2007JAS2412.1.

Reiher, C. A. and A. C. Winters, 2024: Discriminating factors that favor the development of high-impact weather events in association with polar–subtropical jet superpositions. *Mon. Wea. Rev.*, **[submitted]**

Riemer, M., S. C. Jones, C. A. Davis, 2008: The impact of extratropical transition on the downstream flow: An idealized modelling study with a straight jet. *Quart. J. Roy. Meteor. Soc.*, **134**, 69–91, doi: 10.1002/qj.189.

Riemer, M., and S. C. Jones, 2010: The downstream impact of tropical cyclones on a developing baroclinic wave in idealized scenarios of extratropical transition. *Quart. J. Roy. Meteor. Soc.*, **136**, 617–637, doi: 10.1002/qj.605.

Rivière, G., M. Wimmer, P. Arbogast, J.-M. Piriou, J. Delanoë, C. Labadie, Q. Cazenave, and J. Pelon, 2021: The impact of deep convection representation in a global atmospheric model on the warm conveyor belt and jet stream during NAWDEX IOP6. *Weather Clim. Dyn.*, 2, 1011–1031, doi: 10.5194/wcd-2-1011-2021.

Rodwell, M.J., L. Magnusson, P. Bauer, P. Bechtold, M. Bonavita, C. Cardinali, M. Diamantakis, P. Earnshaw, A. Garcia-Mendez, L. Isaksen, E. Kallen, D. Klocke, P. Lopez, T. McNally, A. Persson, F. Prates, and N. Wedi, 2013: Characteristics of occasional poor medium-range weather forecasts for Europe. *Bull. Amer. Meteor. Soc.*, **94**, 1393–1405, doi: 10.1175/BAMS-D-12-00099.1.

Rodwell, M. J., and T. N. Palmer, 2007: Using numerical weather prediction to assess climate models. *Quart. J. Roy. Meteor. Soc.*, **133**, 129–146.

Röthlisberger, M., S. Pfahl, and O. Martius, 2016: Regional-scale jet waviness modulates the occurrence of midlatitude weather extremes. *Geophys. Res. Lett.*, **43**, 10989–10997, doi: 10.1002/2016GL070944.

Röthlisberger, M., O. Martius, and H. Wernli, 2018: Northern hemisphere Rossby wave initiation events on the extratropical jet–A climatological analysis. *J. Climate*, **31**, 743–760, doi: 10.1175/JCLI-D-17-0346.1.

Sanders, F., and J. R. Gyakum, 1980: Synoptic-dynamic climatology of the “bomb”. *Mon. Wea. Rev.*, **108**, 1589–1606, doi: 10.1175/1520-0493(1980)108<1589:SDCOT>2.0.CO;2.

Sanders, F., 1986: Explosive Cyclogenesis over the West-Central North Atlantic Ocean, 1981-84. Part II. Evaluation of LFM Model Performance. *Monthly Weather Review*, **114**, 2207–2218.

Sanders, F., and B. J. Hoskins, 1990: An easy method for estimation of Q-vectors from weather maps. *Wea. Forecasting*, **5**, 346–353, doi: 10.1175/1520-0434(1990)005<0346:AEMFEO>2.0.CO;2.

Schafler, A., and F. Harnisch, 2015: Impact of the inflow moisture on the evolution of a warm conveyor belt. *Quart. J. Roy. Meteor. Soc.*, **141**, 299–310.

Schäfler, A., B. Harvey, J. Methven, J. D. Doyle, S. Rahm, O. Reitebuch, F. Weiler, and B. Witschas, 2020: Observation of jet stream winds during NAWDEX and characterization of systematic meteorological analysis errors. *Mon. Wea. Rev*., **148**, 2889–2907, doi: 10.1175/MWR-D-19-0229.1.

Schwierz, C., M. Croci-Maspoli, and H. C. Davies, 2004: Perspicacious indicators of atmospheric blocking. *Geophysical Research Letters*, **31**, https://doi.org/10.1029/2003GL019341.

Schwierz, C., S. Dirren, and H. C. Davies, 2004: Forced Waves on a Zonally Aligned Jet Stream. *J. Atmos. Sci*, **61**, 73–87. doi: 10.1175/1520-0469(2004)061<0073:FWOAZA>2.0.CO;2

Shapiro, M. A., T. Hampel, and A. J. Krueger, 1987: The arctic tropopause fold. *Monthly Weather Review*, **115**, 444–454.

Shepherd, T. G., I. Polichtchouk, R. J. Hogan, and A. J. Simmons, 2018: Report on stratosphere task force.

Simmonds, I., and I. Rudeva, 2012: The great Arctic cyclone of August 2012. *Geophysical Research Letters*, **39**, https://doi.org/10.1029/2012GL054259.

Solomon, S., and Karen H Rosenlof, Robert W Portman, John S Daniel, Sean M Davis, Todd J Sanford, and Gian-Kasper Plattner, 2010: Contributions of stratospheric water vapor to decadal changes in the rate of global warming. *Science*, **327**, 1219–1223.

Spreitzer, E., R. Attinger, M. Boettcher, R. Forbes, H. Wernli, and H. Joos, 2019: Modification of potential vorticity near the tropopause by nonconservative processes in the ECMWF model. *J. Atmos. Sci.*, 76, 1709–1726, doi: 10.1175/JAS-D-18-0295.1.

Teubler, F., and M. Riemer, 2016: Dynamics of Rossby wave packets in a quantitative potential vorticity–potential temperature framework. *J. Atmos. Sci.*, **73**, 1063–1081.

Thorpe, A. J., 1986: Synoptic scale disturbances with circular symmetry. *Monthly Weather Review*, **114**, 1384–1389.

Tinney, E. M., and C. R. Homeyer, Climatology, sources, and transport characteristics of observed water vapor extrema in the lower stratosphere. *Atmospheric Chemistry and Physics*, **23**, 14375–14392.

Tripathi, O. P., A. Charlton-Perez, M. Sigmond, and F. Vitart, 2015: Enhanced long-range forecast skill in boreal winter following stratospheric strong vortex conditions. *Env. Res. Lett.*, **10**, 104007. doi: 10.1088/1748-9326/10/10/104007

Turner, D. D., M. D. Shupe, and A. B. Zwink, 2018: Characteristic atmospheric radiative heating rate profiles in Arctic clouds as observed at Barrow, Alaska. *Journal of Applied Meteorology and Climatology*, **57**, 953–968.

Uccellini, L. W., P. J. Kocin, R. A. Petersen, C. H. Wash, and K. F. Brill, 1984: The Presidents' Day cyclone of 18–19 February 1979: Synoptic overview and analysis of the subtropical jet streak influencing the pre-cyclogenetic period. *Mon. Wea. Rev.*, **112**, 31–55, doi: 10.1175/1520-0493(1984)112<0031:TPDCOF>2.0.CO;2.

Van Thien, L., W. A. Gallus Jr, M. A. Olsen, and N. Livesey, 2010: Comparison of Aura MLS water vapor measurements with GFS and NAM analyses in the upper troposphere–lower stratosphere. *Journal of Atmospheric and Oceanic Technology*, **27**, 274–289.

Wang, Y., H. Su, J. H. Jiang, N. J. Livesey, M. L. Santee, L. Froidevaux, W. G. Read, and J. Anderson, 2017: The linkage between stratospheric water vapor and surface temperature in an observation-constrained coupled general circulation model. *Climate Dynamics*, **48**, 2671–2683.

Westby, R. M., Y.-Y. Lee, and R. X. Black, 2013: Anomalous temperature regimes during the cool season: Long-term trends, low-frequency mode modulation, and representation in CMIP5 simulations. *J. Climate*, **26**, 9061–9076, doi: 10.1175/JCLI-D-13-00003.1.

Westby, R. M., and R. X. Black, 2015: Development of anomalous temperature regimes over the southeastern United States: Synoptic behavior and role of low-frequency modes. *Wea. Forecasting*, **30**, 553–570, doi: 10.1175/WAF-D-14-00093.1.

Winters, A. C., and J. E. Martin, 2014: The role of a polar/subtropical jet superposition in the May 2010 Nashville flood. *Wea. Forecasting*, **29**, 954–974, doi: 10.1175/WAF-D-13-00124.1.

Winters, A. C., and J. E. Martin, 2016: Synoptic and mesoscale processes supporting vertical superposition of the polar and subtropical jets in two contrasting cases. *Quart. J. Roy. Meteor. Soc.*, **142**, 1133–1149, doi: 10.1002/qj.2718.

Winters, A. C., and J. E. Martin, 2017: Diagnosis of a North American polar–subtropical jet superposition employing piecewise potential vorticity inversion. *Mon. Wea. Rev.*, **145**, 1853–1873, doi: 10.1175/MWR-D-16-0262.1.

Winters, A. C., L. F. Bosart, and D. Keyser, 2019: Antecedent North Pacific jet regimes conducive to the development of continental U.S. extreme temperature events during the cool season. *Wea. Forecasting*, **34**, 393–414, doi: 10.1175/WAF-D-18-0168.1.

Winters, A. C., D. Keyser, L. F. Bosart, and J. E. Martin, 2020a: Composite synoptic-scale environments conducive to North American polar–subtropical jet superposition events. *Mon. Wea. Rev.*, **148**, 1987–2008, doi: 10.1175/MWR-D-19-0353.1.

Winters, A. C., D. Keyser, and L. F. Bosart, 2020b: Composite vertical-motion patterns near North American polar–subtropical jet superposition events. *Mon. Wea. Rev.*, **148**, 4565–4585, doi: 10.1175/MWR-D-20-0140.1.

Winters, A. C., 2021: Kinematic processes contributing to the intensification of anomalously-strong North Atlantic jets. *Quart. J. Roy. Meteor. Soc.*, **147**, [in press], doi: 10.1002/qj.4037.

Winters, A. C. and H. E. Attard, 2022: North Pacific and North Atlantic jet covariability and its relationship to cool season temperature and precipitation extremes. *Wea. Forecasting*, **37**, 1581–1600, doi: 10.1175/WAF-D-21-0203.1.

Winters, A. C. and C. L. Walker, 2022: A jet-centered framework for investigating High Plains winter storm severity. *J. Appl. Meteor. Climatology*, **61**, 709–728, doi: 10.1175/JAMC-D-21-0211.1.

Wirth, V., M. Riemer, E. K. Chang, and O. Martius, 2018: Rossby wave packets on the midlatitude waveguide—A review. *Mon. Wea. Rev.*, **146**, 1965–2001.

Wolter, K., M. Hoerling, J. K. Eischeid, G. J. van Oldenborgh, X.-W. Quan, J. E. Walsh, T. N. Chase, and R. M. Dole, 2015: How unusual was the cold winter of 2013/14 in the Upper Midwest? *Bull. Amer. Meteor. Soc.*, **96**, S10–S14, doi: 10.1175/BAMS-D-15-00126.1.

Woiwode, W., A. Dörnbrack, I. Polichtchouk, S. Johansson, B. Harvey, M. Höpfner, J. Ungermann, and F. Friedl-Vallon, 2020: Technical note: Lowermost-stratosphere moist bias in ECMWF IFS

model diagnosed from airborne GLORIA observations during winter–spring 2016. *Atmos. Chem. Phys.*, **20**, 15379–15387, doi: 10.5194/acp-20-15379-2020.

Wong, M., G. Romine, and C. Snyder, 2020: Model improvement via systematic investigation of physics tendencies. *Monthly Weather Review*, **148**, 671–688.

Xi, X., D. Steinfeld, S. M. Cavallo, J. Wang, J. Chen, K. Zulpykharov, and G. M. Henebry, 2023: What caused the unseasonal extreme dust storm in Uzbekistan during November 2021? *Environmental Research Letters*,.

Xie, Z., R. X. Black, and Y. Deng, 2017: Daily-scale planetary wave patterns and the modulation of cold season weather in the northern extratropics. *J. Geophys. Res. Atmos.*, **122**, 8383– 8398, doi: 10.1002/2017JD026768.

Yamagami, A., M. Matsueda, and H. L. Tanaka, 2017: Extreme Arctic cyclone in august 2016. *Atmospheric Science Letters*, **18**, 307–314.

Zhang, J., R. Lindsay, A. Schweiger, and M. Steele, 2013: The impact of an intense summer cyclone on 2012 Arctic sea ice retreat. *Geophysical Research Letters*, **40**, 720–726, https://doi.org/10.1002/grl.50190.

Zhang, F., N. Bei, R. Rotunno, C. Snyder, and C. C. Epifanio, 2007: Mesoscale predictability of moist baroclinic waves: Convection-permitting experiments and multistage error growth dynamics. *J. Atmos. Sci.*, **64**, 3579–3594.